nature methods

ARTICLES

https://doi.org/10.1038/s41592-020-0936-3

An expanded palette of dopamine sensors for multiplex imaging in vivo

Tommaso Patriarchi[1,6,7,9], Ali Mohebi[2,9], Junqing Sun[1,3,8,9], Aaron Marley[4], Ruqiang Liang[1], Chunyang Dong[1], Kyle Puhger[3], Grace Or Mizuno[1], Carolyn M. Davis[1], Brian Wiltgen[3], Mark von Zastrow[4,5]✉, Joshua D. Berke[2,5]✉ and Lin Tian[1]✉

Genetically encoded dopamine sensors based on green fluorescent protein (GFP) enable high-resolution imaging of dopamine dynamics in behaving animals. However, these GFP-based variants cannot be readily combined with commonly used optical sensors and actuators, due to spectral overlap. We therefore engineered red-shifted variants of dopamine sensors called RdLight1, based on mApple. RdLight1 can be combined with GFP-based sensors with minimal interference and shows high photostability, permitting prolonged continuous imaging. We demonstrate the utility of RdLight1 for receptor-specific pharmacological analysis in cell culture, simultaneous assessment of dopamine release and cell-type-specific neuronal activity and simultaneous subsecond monitoring of multiple neurotransmitters in freely behaving rats. Dual-color photometry revealed that dopamine release in the nucleus accumbens evoked by reward-predictive cues is accompanied by a rapid suppression of glutamate release. By enabling multiplexed imaging of dopamine with other circuit components in vivo, RdLight1 opens avenues for understanding many aspects of dopamine biology.

A recent advance in the measurement of neuromodulators was the development of optical sensors such as dLight1 and $GRAB_{DA}$, which are intensity-based, genetically encoded indicators for dopamine (DA) and have high molecular specificity[1,2]. These sensors bridge the temporal scales of microdialysis and voltammetry by permitting prolonged detection of behaviorally relevant DA fluctuations with high spatial and temporal resolution. Dissemination of, for example, dLight1 has already facilitated discoveries about behavioral conditions and neural mechanisms controlling DA release[3,4].

Our understanding of how neuromodulators are regulated, and how they influence neural circuits, could be enhanced by combining these sensors with optical measurements of other circuit components. Multiplexed imaging became possible with the introduction of red-shifted genetically encoded calcium indicators[5], which have increasingly been optimized for improved sensitivity and brightness[6]. Non-genetically encoded red-shifted probes for DA imaging based on single-walled carbon nanotubes have been developed, yet their application is currently limited to cultured cells or brain slices[7,8].

Here, we expand the color spectrum of dLight1 to introduce both yellow- and red-sensor variants (termed YdLight1.1 and RdLight1, respectively). In HEK293 cells, we establish an in vitro assay for optical dissection of drug efficacy at two distinct DA-receptor subtypes using RdLight1 and dLight1.5. In striatal slices, we characterize the sensitivity and kinetics of RdLight1 in response to endogenous DA release triggered by electrical stimuli. Finally, we demonstrate multicolor photometry through a single optic fiber in the nucleus accumbens (NAc) of awake behaving rats, compare DA release to postsynaptic neuronal activity in cells with DA D1 receptors and compare DA and glutamate dynamics in response to reward-predictive cues (Extended Data Fig. 1).

Results

Sensor engineering. To obtain a yellow-shifted DA sensor, named YdLight1, we introduced two point mutations in dLight1.3b (V284Y/S397A, corresponding to V203Y/S72A mutations in enhanced GFP (eGFP)) that have previously been shown to yellow-shift the excitation and emission properties of eGFP[9–11] (Fig. 1a and Extended Data Fig. 2a). When expressed in HEK cells, YdLight1 showed a ~12-nm right-shift in the emission peak (525 nm) compared with its parent sensor (Fig. 1b), while maintaining membrane expression and a strong positive response to bath-applied DA (averaged fluorescence fold-change, $\Delta F/F = 306 \pm 14\%$ (mean ± s.e.m.); Fig. 1c,d). To generate a red DA sensor, we replaced circularly permuted GFP in dLight1.3b with cpmApple and its flanking linker sequences, derived from jRGECO1a (Fig. 1a)[6]. Though it was well expressed on the membrane, the initial variant (LSSPV-cpmApple-DQDDL) showed no response to DA (Extended Data Fig. 2b). To improve DA sensitivity, we generated a linker library flanking both sides of cpmApple. Of a total of 264 variants screened, we identified a variant with a strong positive fluorescence response to bath-applied DA (Extended Data Fig. 2c). We then mutated residue F129, which we had previously discovered as a site capable of tuning the fluorescence responses of dLight1 (ref. [1]), to a selected set of amino

[1]Department of Biochemistry and Molecular Medicine, University of California, Davis, Sacramento, CA, USA. [2]Department of Neurology, University of California, San Francisco, San Francisco, CA, USA. [3]Center for Neuroscience, University of California, Davis, Davis, CA, USA. [4]Department of Psychiatry, University of California, San Francisco, San Francisco, CA, USA. [5]Weill Institute for Neurosciences and Kavli Center for Fundamental Neuroscience, University of California, San Francisco, San Francisco, CA, USA. [6]Present address: Institute of Pharmacology and Toxicology, University of Zurich, Zurich, Switzerland. [7]Present address: Neuroscience Center Zurich, University and ETH Zurich, Zurich, Switzerland. [8]Present address: Key Laboratory of Medical Electrophysiology, Institute of Cardiovascular Research, Southwest Medical University, Luzhou, China. [9]These authors contributed equally: Tommaso Patriarchi, Ali Mohebi, Junqing Sun. ✉e-mail: mark@vzlab.org; Joshua.Berke@ucsf.edu; lintian@ucdavis.edu

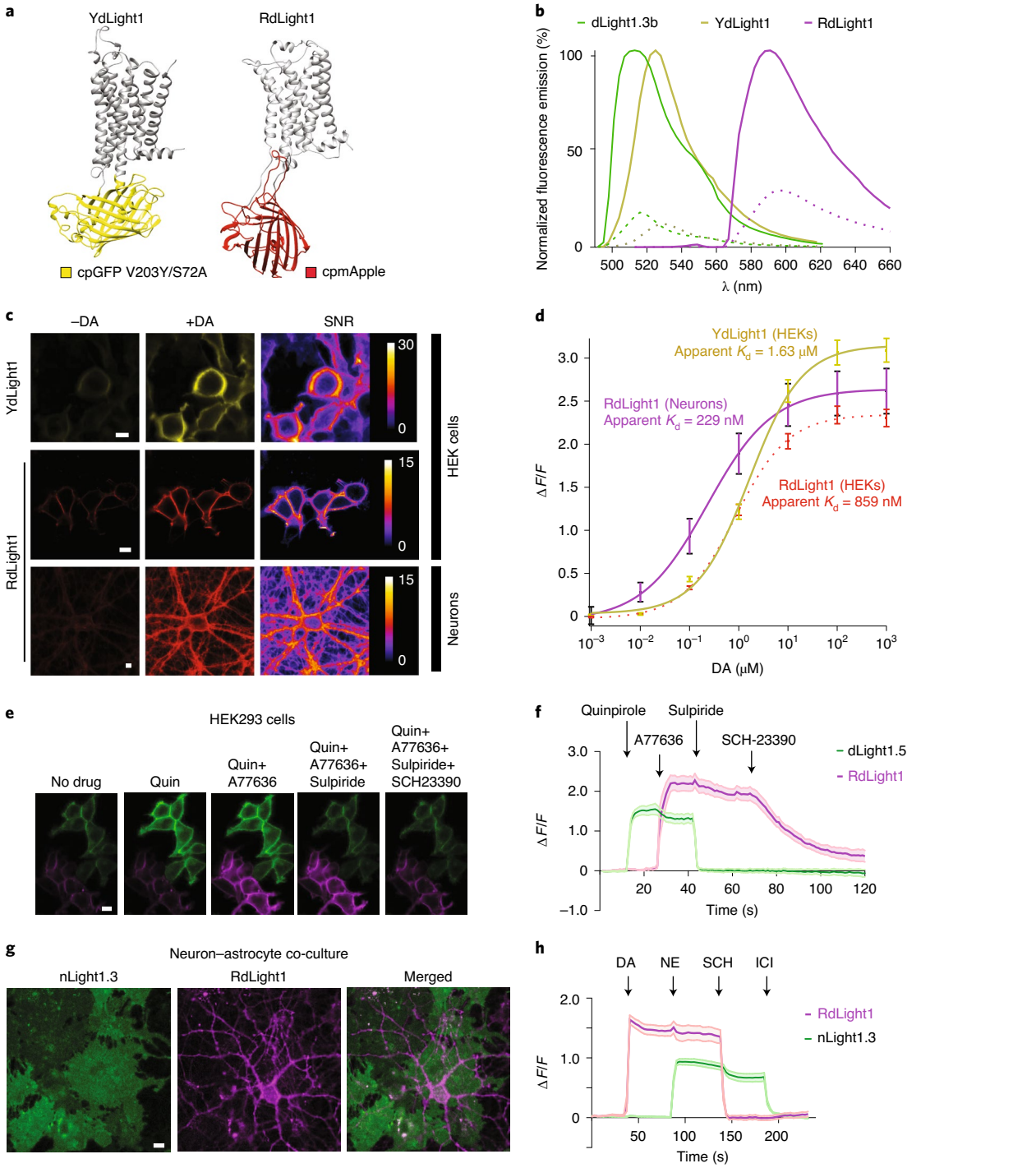

Fig. 1 | Engineering and characterization of red-shifted dLight1 variants. a, Simulated structure of yellow and red DA sensors. **b**, Emission spectra of dLight1.3b, YdLight1 and RdLight1. The fluorescence emission was measured in HEK293 cells before (dotted lines) and after (continuous lines) addition of 100 μM DA to the medium. **c**, In vitro characterization of dLight1.3b spectral variants. Representative images showing expression and fluorescence response of YdLight1 and of RdLight1 in HEK293 cells and dissociated hippocampal neurons. SNR heatmaps were calculated on the basis of the response to 100 μM DA. $n = 3$ cells from 3 separate experiments. Scale bars, 10 μm. **d**, In situ titration of DA on HEK293 cells. Apparent affinity values (apparent K_d) are defined as the concentration of the ligand producing 50% of maximal fluorescence changes (max $\Delta F/F$). YdLight1, apparent $K_d = 1.63 \pm 0.26$ μM ($n = 9$ cells); RdLight1, apparent $K_d = 859 \pm 7$ nM ($n = 26$ cells) in HEK293 cells and 229 ± 2 nM ($n = 15$ cells) in neurons. Data are shown as mean ± s.e.m. **e**,**f**, Multiplex imaging of drug efficacy at distinct DA-receptor subtypes. **e**, representative images of HEK293 cells expressing either dLight1.5 or RdLight1 and their average fluorescent responses to individual drugs. Scale bars, 10 μm. **f**, Fluorescence responses of both sensors in **e** during drug application are shown. Maximal fluorescent responses: green channel after quinpirole (10 μM) ($\Delta F/F = 155 \pm 14\%$), red channel after A77636 (100 nM) ($\Delta F/F = 221 \pm 19\%$), green channel after sulpiride (400 nM) ($\Delta F/F = 1 \pm 3\%$), red channel after SCH-23390 (10 μM) ($\Delta F/F = 32 \pm 17\%$). $n = 6$ cells from 3 cultures. Data are shown as mean ± s.e.m. **g**, Multiplexed imaging in neuron–astrocyte coculture. Cells were transduced with AAV1.*GFAP*.nLight1.3 and AAV.*hSynapsin1*.RdLight1 14 d prior to imaging for selective expression of nLight1.3 in astrocytes and RdLight1 in neurons. Representative images of sensor-expressing cells are shown. $n = 3$ cells from 3 separate experiments. Scale bar, 10 μm. **h**, Fluorescence responses of cells in **g** to bath-applied DA, NE, SCH-23390 (SCH) and ICI118551 (ICI) (1 μM of all drugs). $n = 3$ cells from 3 separate experiments. mean ± s.e.m.

acids. The F129E variant showed excellent membrane expression and fluorescence response ($\Delta F/F = 248 \pm 7\%$), and we thus named this variant RdLight1 (Extended Data Fig. 2d). The emission spectrum measured in HEK293 cells expressing RdLight1 peaks at ~588 nm, with minimal overlap with dLight1.3b (Fig. 1b). We tested the variant for photoactivation upon blue-light illumination[6] in HEK293 cells, and found that continuous or burst illumination at 488 nm elicited a negligible increase of fluorescence intensity compared with that of DA-induced fluorescence changes (Extended Data Fig. 3).

Intrinsic properties of RdLight1. In situ titrations of DA onto YdLight1- and RdLight1-expressing HEK cells or dissociated hippocampal neurons revealed apparent affinities of the sensors in the physiological range (Fig. 1c,d). RdLight1 is ~350 and ~60 times more sensitive to DA than to norepinephrine (NE) in neurons and HEK293 cells, respectively; the maximal response of RdLight1 to NE at 100 µM and above was substantially lower than that to DA (Extended Data Fig. 4a,b). We observed negligible responses to all other tested neurotransmitters (acetylcholine, glutamate, serotonin, histamine), except for epinephrine at high concentrations (≥10 µM) (Extended Data Fig. 4c).

RdLight1 is effectively inert with respect to engagement of endogenous G-protein- or β-arrestin-mediated signaling mechanisms. In HEK293 cells expressing wild-type D1 receptors, application of the D1 agonist SKF81297 markedly increased cAMP production, indicative of receptor signaling by coupling to stimulatory G proteins (Extended Data Fig. 5a). In contrast, in cells expressing RdLight1, D1 agonist produced no increase above the baseline level observed in GFP-expressing negative control cells (Extended Data Fig. 5a). RdLight1 also does not block G-protein signaling, because it had no detectable effect on the cAMP response measured in U2OS cells that express D1 endogenously[1] (Extended Data Fig. 5b), and it did not produce any detectable effect on the cAMP response mediated by endogenous D1 in cultured striatal neurons, which express endogenous D1 in ~50% of cells[12] (Extended Data Fig. 5c). We next confirmed that RdLight1 does not engage β-arrestins. Using live-cell total internal reflection fluorescence microscopy to measure agonist-induced receptor internalization, an indicator of receptor binding to endogenous β-arrestins[13], Flag-tagged RdLight1 remained in the plasma membrane whereas Flag-tagged D1 rapidly internalized (Extended Data Fig. 5d,e). We independently verified the lack of β-arrestin engagement with RdLight1 by measuring surface recruitment of GFP-tagged β-arrestin-2, which is a highly sensitive assay capable of detecting even weak or transient G-protein-coupled receptor (GPCR) interactions with β-arrestin[13]. Whereas D1 robustly mediated agonist-dependent recruitment of β-arrestin into puncta at the plasma membrane, RdLight1 did not (Extended Data Fig. 5f–i).

Dual-color imaging in cells. A major advantage enabled by red-shifted probes is their combination with GFP-based reporters in multiplexed imaging experiments[5]. We leveraged this to distinguish spectrally orthogonal probes pharmacologically. As the GFP-based dLight1.5 is a DRD2-based DA sensor, and is spectrally distinct from the D1-based RdLight1 (Extended Data Fig. 6a), we examined the feasibility of simultaneously monitoring responses to subtype-selective drugs. We combined two populations of HEK cells expressing dLight1.5 or RdLight1, which was followed by dual-color confocal imaging. Bath application of a selective D2 agonist (quinpirole) led to a green-fluorescence increase of dLight1.5, but failed to elicit any response from RdLight1 (Fig. 1e,f). Subsequent application of a selective D1 agonist (A77636) led to a fluorescence increase of RdLight1, but not of dLight1.5. In fact, A77636 slightly decreased dLight1.5 fluorescence in the combined presence of quinpirole (Fig. 1e,f), an observation consistent with A77636 having weak partial agonist activity at D2 receptors[14]. Concentration–response curves of each agonist emphasized the high degree of pharmacological selectivity that can be achieved using this multiplex detection strategy (Extended Data Fig. 6b,c). Furthermore, application of subtype-selective antagonists brought the green (sulpiride) or red (SCH-23390) fluorescence from the peak to the baseline (Fig. 1e,f and Supplementary Movie 1).

As RdLight1 selectively responds to DA in neurons, we next tested whether combining RdLight1 with a β_2-adrenergic receptor (β_2AR)-based NE sensor (nLight1.3)[15] would allow these two catecholamines to be optically dissected from each other with high molecular specificity. We used a neuron–astrocyte coculture system to selectively infect neurons and astrocytes with RdLight1 (AAV9.*hSynapsin1*.RdLight1) and nLight1.3 (AAV1.*GFAP*.nLight1.3), respectively, using tissue-specific promoters to maximize expression of both sensors (Fig. 1g). We chose to separate expression of the sensors in different cell populations to avoid possible interference or interaction between sensors (Extended Data Fig. 6d–f). We then performed time-lapse, dual-color imaging during sequential bath application of 1 µM DA, 1 µM NE, the D1 antagonist SCH-23390 (for RdLight1) and the β_2AR antagonist ICI118551 (for nLight1.3). We observed cell-type-specific responses to application of each catecholamine, and reversal by receptor-specific antagonists (Fig. 1h and Supplementary Movie 2).

Simultaneous imaging of DA and glutamate or intracellular calcium transients ex vivo. We next examined the sensitivity of RdLight1 to endogenous DA release using two-photon imaging in striatal slices (Fig. 2a). We infected the dorsal striatum of young mice (8–12 weeks old) with AAV9.*hSynapsin1*.RdLight1 and allowed 2–4 weeks for expression before acute slice preparation. Upon application of a brief electrical stimulus (0.5 ms), frame scans at high frequency (198 Hz) revealed a rapid fluorescent response with kinetics similar to those previously described for dLight1 (Fig. 2b). RdLight1 robustly reported DA release triggered by electrical stimuli, which we repeated over the course of continuous two-photon imaging, though the baseline fluorescence declined about 17% at the end of the imaging session (Extended Data Fig. 7). When we applied a selective DA-reuptake blocker (1 µM GBR12909) to the slice, the decay time of the electrically evoked DA transient was significantly increased (*$P = 0.009$, paired *t*-test (two-sided)), whereas application of a D1-selective antagonist (10 µM SKF83566) completely blocked the response (Fig. 2c,d).

A palette of neurotransmitter sensors offers the potential for monitoring multiple transmitters simultaneously at the same location. As the striatum receives both dopaminergic and glutamatergic inputs, we next tested whether we could separately image evoked DA and glutamate transients. We coinjected RdLight1 with the glutamate sensor iGluSnFR[16] (AAV5.*hSynapsin1*.iGluSnFR). We observed a diffuse expression pattern in both green and red channels, which is consistent with the expression pattern of membrane-localized sensors[1,16,17] (Fig. 2e). In response to a single pulse of electrical stimulation, two-photon frame scans revealed fluorescence changes in both green and red channels, with distinct peak amplitudes and decay kinetics (Fig. 2f). To further confirm molecular specificity, we applied the excitatory amino acid transporter-2 (EAAT-2) selective blocker (WAY213613, 20 µM), which selectively increased the decay time of the iGluSnFR response (*$P = 0.005$, paired *t*-test (two-sided)), but not its peak amplitude ($P = 0.798$, paired *t*-test (two-sided)) (Fig. 2f,g). We did not observe significant changes in either the decay time ($P = 0.123$ paired *t*-test (two-sided)), or the amplitude ($P = 0.093$, paired *t*-test (two-sided)) of the simultaneously recorded response of RdLight1 with the addition of WAY213613 (Fig. 2f,g, $P > 0.05$).

As a final ex vivo experiment, we tested whether multiplexed imaging can simultaneously visualize both local DA transients

and neuronal activity. We coinjected RdLight1 with GCaMP6s[18] (AAV1.*hSynapsin1*.GCaMP6s) in the striatum. Two to three weeks later, the expression pattern of each sensor could be distinguished by two-photon imaging: GCaMP6s-labeled neuronal somata whereas RdLight1 outlined the membrane (Fig. 2h). A train of 20 pulses applied at 40 Hz triggered responses from both indicators, and the decay kinetics of calcium transients and DA release were clearly distinct (*$P = 0.0002$, paired *t*-test (two-sided)) (Fig. 2i,j). Therefore, multiplexed imaging of neurotransmitters and cell-type-specific neural activity can be achieved by combining RdLight1 with other GFP-based sensors.

Multiplex measurements of DA release with cell-type-specific input and output activity in vivo. To assess the utility of RdLight1 in vivo, we first examined the response of RdLight1 to DA changes in the nucleus accumbens (NAc) triggered by optical stimulation of midbrain DA neurons in freely behaving rats. In TH-Cre rats[19], we infected the ventral tegmental area (VTA) with AAV.*EF1a*.FLEX.ChR2.EYFP[4,20] and the NAc with AAV9.*CAG*.RdLight1 (Fig. 3a and Extended Data Fig. 8). Using chronically implanted optical fibers, we monitored the RdLight1 photometry signal in the NAc while delivering laser pulses in the VTA to evoke DA release (Fig. 3b)[21]. RdLight1 showed clear, frequency-dependent DA increases in response to optical stimulation, with individual peaks of pulse-evoked DA transients visible at up to 8 Hz (Fig. 3b).

We next performed simultaneous measurements of presynaptic activity in DA terminals (using GCaMP6f) and the resulting DA release. In TH-Cre rats, we infected the VTA with Cre-dependent, axon-targeted GCaMP6f (AAV1.*hSynapsin1*.FLEX.axonGCaMP6f (ref. [22])) and the NAc with RdLight1 (AAV9.CAG.RdLight1), then recorded dual-color photometry signals through a single optic fiber in the NAc (Fig. 3c–g and Extended Data Fig. 8). Rats were freely moving within an operant chamber, and uncued sugar-pellet rewards were delivered at random intervals (with an audible click of the food hopper). RdLight1 displayed minimal photobleaching over the long duration of these experiments (Fig. 3c) with consistent signal changes to unpredicted rewards. Reward delivery evoked rapid increases in both GCaMP6f and RdLight1 signals, with a similar time course (Fig. 3d,e). The session-wide cross-correlation between presynaptic calcium and DA release was strong (peak cross-correlation = 0.86) (Fig. 3f,g) without appreciable lag, suggesting high fidelity between pre- and postsynaptic measurements of DA release.

The nature of DA's influence in the NAc is not fully understood, in part because distinct cell subpopulations express different DA receptors. We therefore tested whether Rdlight1 can simultaneously resolve DA fluctuations and the activity dynamics of genetically specified postsynaptic subpopulations in behaving animals. We took advantage of a recently developed CRISPR knock-in rat that expresses Cre recombinase in D1-receptor-expressing cells[23], and injected into the NAc both RdLight1 (AAV9.*CAG*.RdLight1) and Cre-dependent GCaMP6f (AAV5.*hSynapsin1*.FLEX.GCaMP6f; Fig. 3h and Extended Data Fig. 8). Once again, unexpected rewards were followed by increases in both signals, but this time there was a clear difference in time course (Fig. 3i). Throughout the session, calcium in $D1^+$ cells correlated with, but lagged behind, DA signals (Fig. 3j,k; peak cross-correlation = 0.54, at +372 ms).

Multiplexed measurement of DA and glutamate release in vivo. We next assessed our ability to study multiple, interacting neurotransmitters through the same optic fiber in behaving animals. The NAc receives glutamatergic input from multiple sources, and NAc DA terminals can also corelease glutamate[24], but the relative timing of DA and glutamate signals at fast timescales is unknown. In wild-type rats we coinjected RdLight1 (AAV9.*CAG*.RdLight1) and iGluSnFR (AAV1.*hSynapsin1*.iGluSnFR*)* into NAc, and chronically implanted an optic fiber (Fig. 4a and Extended Data Fig. 8). Aligned to an unpredicted reward cue, we again observed increased DA release (Fig. 4b, bottom); for glutamate, we instead observed a strong decline in signal after a brief delay (Fig. 4b, top). DA increases to the reward cue were attenuated when the reward cue was partly predicted by preceding cues, as previously reported for dLight1 signals[1,4]. Consistent with reward-prediction-error coding by DA[25], these preceding cues themselves evoked DA release, in proportion to the likelihood of reward that they signaled (Fig. 4c, bottom). These cues also produced glutamate dips that scaled with DA increases (Fig. 4c, top). The correspondence between fast DA increases and slightly delayed and slower glutamate dips is consistent with a known mechanism of DA action at D2 receptors on presynaptic glutamate terminals to suppress release[26], but to our knowledge has not been previously reported in behaving animals.

In separate animals, we performed two control experiments to exclude the possibility that decreases in iGluSnFR signals were the result of cross-talk caused by RdLight1 coexpression. First, we injected iGluSnFR alone (AAV1.*hSynapsin1*.iGluSnFR*)*, and again observed a decrease in NAc iGluSnFR signal in response to unpredicted reward cues (Extended Data Fig. 9a–c). Next, we coinjected RdLight1 (AAV9.*CAG*.RdLight1) and a mutated iGluSnFR with ablated glutamate binding (AAV1.*hSynapsin1*.iGluSnFR(mut))

Fig. 2 | Two-photon imaging of RdLight1 in acute brain slices. a, Schematic representation of viral injection in dorsal striatum of mice (left), and representative image of RdLight1 expression in the striatum from a SeeDB[46] cleared brain slice (right, $n = 2$ mice). Scale bar, 1 mm. **b**, Single-trial fluorescence response (average in black) of RdLight1 to a single stimulus (4 V, 0.5 ms), acquired at 198 Hz. $\Delta F/F = 20.2 \pm 1.8\%$ across 7 trials in 3 mice, $tau_{on} = 14.1 \pm 1.5$ ms (rise time from application of stimulus to maximal $\Delta F/F$) and $tau_{off} = 0.398 \pm 0.058$ s (exponential decay time from maximal $\Delta F/F$ to baseline), mean ± s.e.m. The inset shows a zoomed-in view of the fluorescence peak. **c**, Single-trial fluorescence responses (average in black) of RdLight1 in response to a single stimulus (4 V, 0.5 ms) in the presence of GBR12909 (1 µM, $tau_{off} = 3.580 \pm 0.764$ s) or SKF83566 (10 µM), acquired at 30 Hz. $n = 7$ trials from 4 mice. **d**, Quantification $\Delta F/F$ and decay time in **c**. Peak fluorescence: no drug, 21.7 ± 2.8%; GBR12909, 22.2 ± 2.0%; $P = 0.800$, paired *t*-test (two-sided). Decay time: no drug, 0.560 ± 0.076 s; GBR12909, 3.580 ± 0.764 s; *$P = 0.009$, paired *t*-test (two-sided). $n = 7$ trials from 4 mice, mean ± s.e.m. **e**, Representative histology images of iGluSnFR and RdLight1 expression ($n = 2$ mice). Scale bar, 0.5 mm or 20 µm. **f**, Fluorescence responses (average in black from 5 trials of 3 mice) of simultaneously recorded iGluSnFR and RdLight1 to electrical stimulation (5 pulses, 4 V, 0.2 ms at 40 Hz) before and during application of WAY213613 (20 µM). RdLight1, $\Delta F/F = 19.4 \pm 3.0\%$, $tau_{off} = 0.611 \pm 0.288$ s; iGluSnFR, $\Delta F/F_{max} = 63.3 \pm 12.8\%$, $tau_{off} = 0.100 \pm 0.024$ s. Images acquired at 30 Hz. **g**, Quantification of decay time and $\Delta F/F$ for the responses in **f**. For iGluSnFR, decay time in no drug: 0.100 ± 0.024 s, with WAY213613: 0.792 ± 0.129 s, *$P = 0.005$, paired *t*-test (two-sided); peak fluorescence in no drug: 63.3 ± 12.8%, with WAY213613: 66.3 ± 5.4%, $P = 0.798$, paired *t*-test (two-sided). For RdLight1, decay time in no drug: 0.611 ± 0.288 s, with WAY213613: 1.093 ± 0.409 s, $P = 0.123$, paired *t*-test (two-sided); peak fluorescence in no drug: 19.4 ± 3.0%, with WAY213613: 16.7 ± 3.5%, $P = 0.093$, paired *t*-test (two-sided). $n = 5$ trials from 3 mice, mean ± s.e.m. **h**, Representative histology images of RdLight1 and GCaMP6s expression ($n = 2$ mice). Scale bar, 0.5 mm or 20 µm. **i**, Representative single-trial fluorescence responses (average in black, from 17 trials of 10 mice) of simultaneously recorded GCaMP6s and RdLight1 in response to electrical stimulation (20 pulses, 4 V, 0.2 ms at 40 Hz). Images acquired at 30 Hz. **j**, Quantification of decay time response in **i**. GCaMP6s: 1.202 ± 0.061 s; RdLight1: 0.778 ± 0.055 s. *$P = 0.0002$, paired *t*-test (two-sided). $n = 17$ trials from 10 mice, mean ± s.e.m.

in the NAc. This time, we again observed a robust increase in the RdLight1 signal, but no apparent increase in fluorescence intensity in the iGluSnFR(mut) signal (Extended Data Fig. 9d–f).

To provide additional support for these observations, and to also begin distinguishing between distinct glutamate inputs to the NAc, we expressed axon-targeted GCaMP6f (AAV1.*hSynapsin1*.

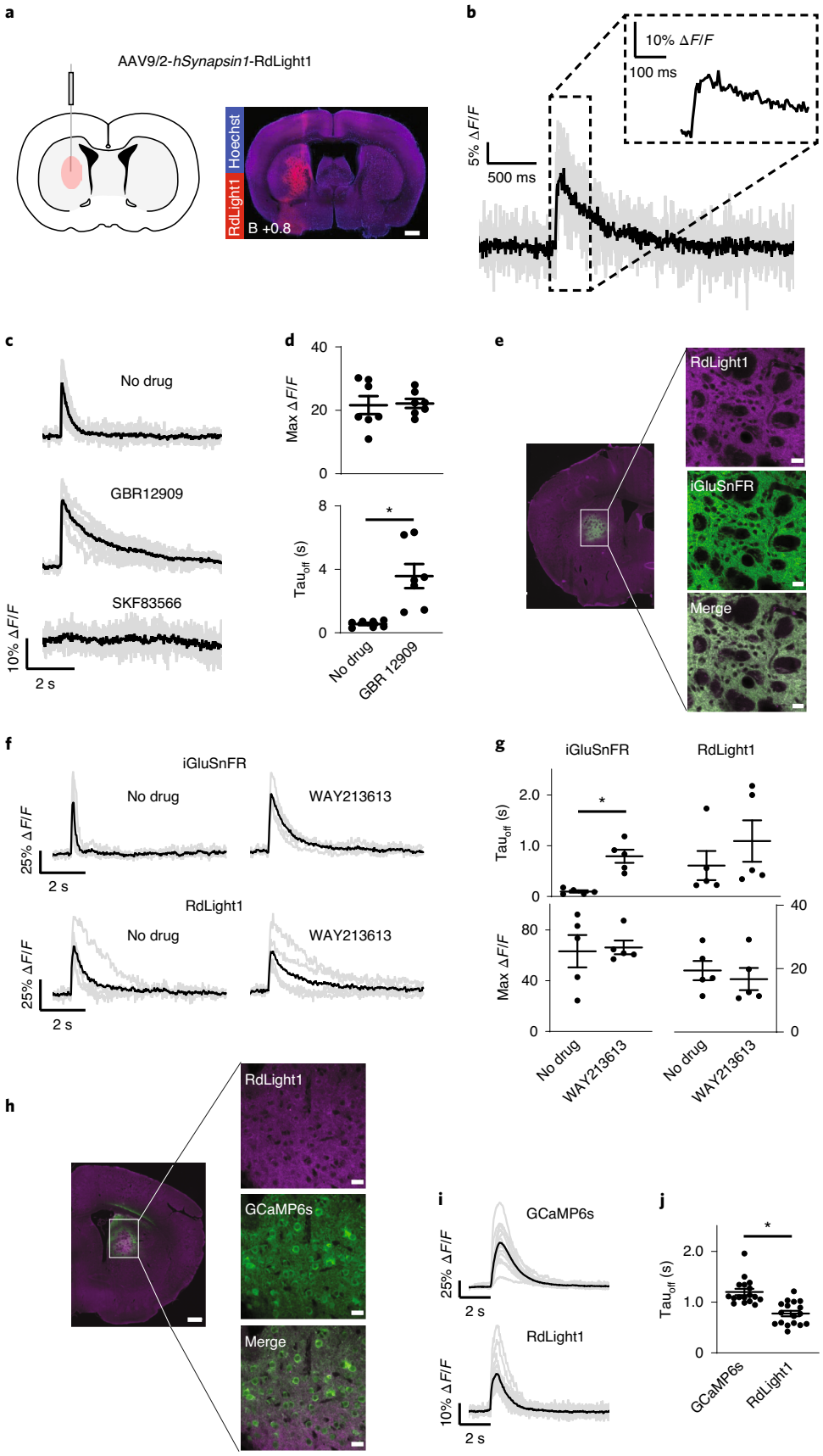

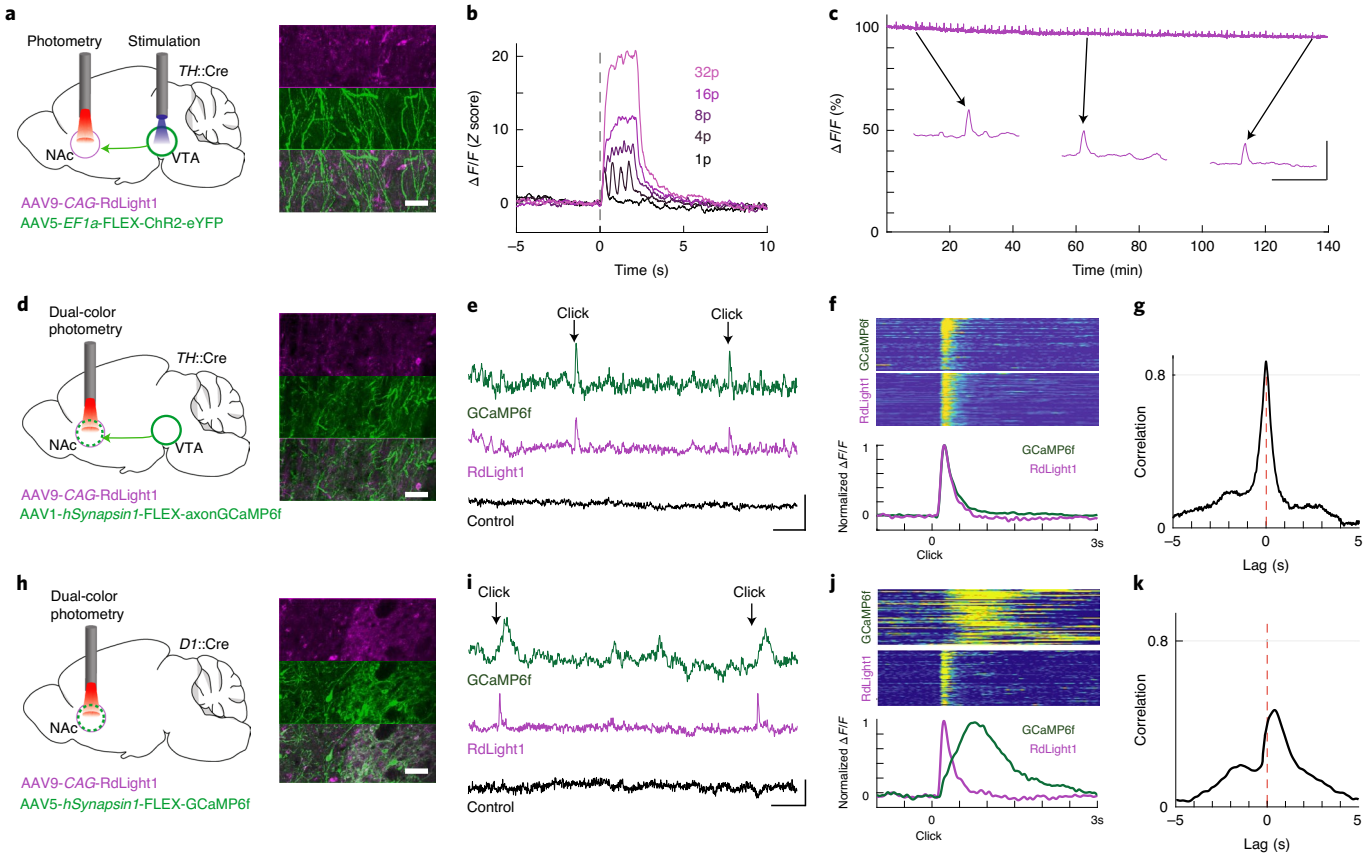

Fig. 3 | Combining RdLight1 with optogenetics and calcium monitoring in vivo. a, Left, schematic representation of viral injections and fiber implants in the NAc and VTA, using TH-Cre rats and Cre-dependent virus to drive ChR2 expression selectively in DA neurons. Right, representative micrograph showing RdLight1 in red and ChR2-eYFP in green ($n=2$ rats). Scale bar, 50 µm. **b**, Mean fluorescence changes of RdLight1 across all trials ($n=250$ trials) in the NAc, produced by blue-light (462 nm, 10 mW at fiber tip) stimulation of VTA. Light pulses were 2 ms in duration and given as either a single pulse (1p) or a 2-s-duration train with the indicated number of pulses. **c**, Single-trial fluorescence changes of RdLight1 over prolonged monitoring in vivo. The rat was given 60 rewards at unpredictable times over a >2-h period. Individual reward responses are shown in the insets. At 2 h, fluorescence = 95.3 ± 0.034% (mean ± s.e.m.) of starting fluorescence ($n=4$ rats); inset scale bars, 5 ms, 5% $\Delta F/F$. **d**, Left, schematic of dual-color photometry, again in TH-Cre rats but this time using virus to drive axon-targeted GCaMP6f in DA terminals. Right, representative micrograph showing RdLight1 in red and axon-GCaMP6f in green ($n=2$ rats). Scale bar, 50 µm. **e**, Single-trial fluorescence ($n=60$ trials) changes from simultaneous recording of RdLight1 555–570 nm and 580–680 nm (excitation and emission), GCaMP6f 460–490 nm and 500–540 nm (excitation and emission) and isosbestic (non-calcium-dependent) 400–410 nm and 500–540 nm (excitation and emission) control around unexpected, audible reward deliveries ('Clicks' of the food hopper). Scale bars, 6 s, 5% $\Delta F/F$. **f**, Top, fluorescence changes of all trials ($n=60$ trials) of unexpected reward deliveries. Yellow, maximum. Bottom, mean fluorescence changes across all trials ($n=120$ trials from two rats). RdLight1 $tau_{on} = 126 \pm 15$ ms and $tau_{off} = 320 \pm 42$ ms, mean ± s.e.m. Tau_{on} was calculated by fitting this average RdLight1 fluorescence rise with a linear regression, and tau_{off} was calculated by fitting the fluorescence decay with a single exponential curve. **g**, Session-wide cross-correlation between presynaptic calcium in DA terminals and DA release. Peak correlation = 0.86 ± 0.06 at zero lag ($n=2$ sessions). **h**–**k**, Data are as described in **c**–**f**, but with GCaMP6f expressed in D1$^+$ cells (in D1-Cre rats). Session-wide cross-correlation (average of two rats) between RdLight1 and GCaMP6f. Peak correlation = 0.54 at a lag of 372 ms (DA leading). Scale bar, 50 µm.

axonGCaMP6f) in the medial prefrontal cortex, and then carried out simultaneous RdLight1 and GCaMP6f photometry in the NAc (Fig. 4d). We observed a very similar activity pattern in medial prefrontal cortex (mPFC) axons to the local glutamate dynamics described above (Fig. 4e,f), indicating that mPFC terminals in the NAc are participating in the general suppression of glutamate transmission that accompanies DA release after reward-predictive events.

Finally, we compared the peak signal-to-noise ratio (SNR) of RdLight1 to unpredicted rewards with green dLight1.3b, which displays the highest dynamic range in the dLight1 family. We noticed that the SNR of RdLight1 was significantly higher than that of dLight1.3b (approximately twofold, $P = 8 \times 10^{-3}$, one-sided t-test; Extended Data Fig. 10a). In addition, in a motivated behavior that is sensitive to NAc DA[27], the time taken to approach rewards did not differ between uninjected rats and those expressing either dLight1.1 or RdLight1 in the NAc (Extended Data Fig. 10b), suggesting that overexpression of RdLight1 does not appreciably affect NAc function in vivo.

Discussion

As the toolbox of genetically encoded optical sensors continues to grow, combining these tools becomes an increasingly powerful approach for dissecting information processing within brain circuits. To date, the useful red-shifted sensors for in vivo imaging are jRGECO and jRCaMP, which severely restricts the number of signaling events that can be studied simultaneously. Here, we expanded the color spectrum of dLight1 by introducing two new spectral variants, the yellow YdLight1 and the red RdLight1. Though the utility of YdLight1 in multiplex imaging may be limited, it could

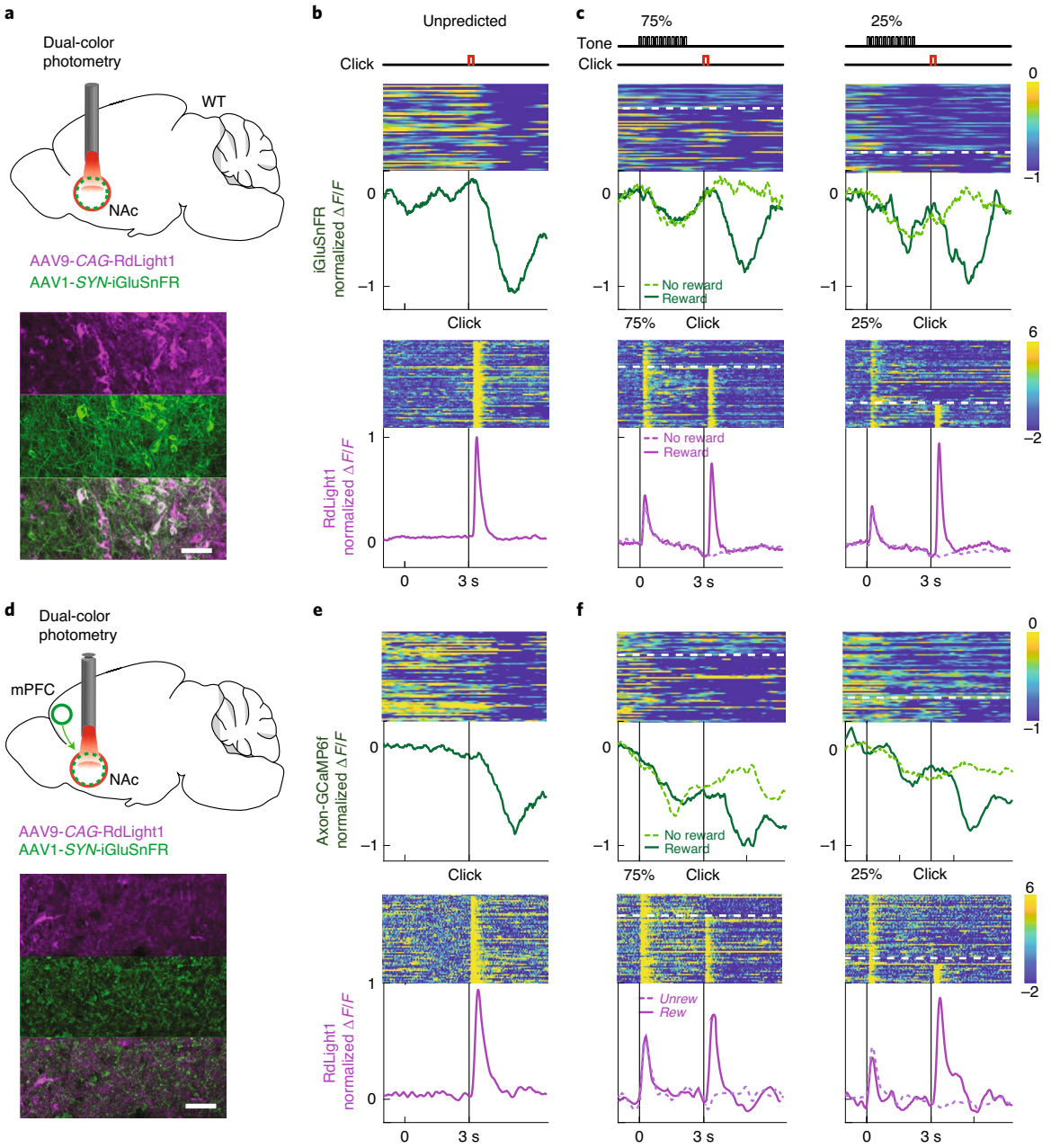

Fig. 4 | Combining RdLight1 with glutamate monitoring in vivo. a, Top, schematic representation of dual-color photometry in the NAc of wild-type rats coexpressing RdLight1 and iGluSnFR injected in the NAc. Bottom, example micrograph showing RdLight1 in red and iGluSnFR in green. Scale bar, 50 µm. **b**, iGluSnFR- and RdLight1-signal changes in the NAc following unpredicted reward delivery. Top, fluorescence changes to unexpected reward deliveries in all trials ($n = 60$ trials). Bottom, mean fluorescence changes across all trials ($n = 120$ trials of 2 rats). **c**, Tones (of different frequencies) signaled availability of reward delivery with different probabilities (75% or 25%) after a fixed period of 3 s. Solid and dotted lines indicate rewarded and unrewarded trials, respectively, for iGluSnFR in green and RdLight1 in red. Top, fluorescence changes in response to unexpected reward deliveries in all trials ($n = 60$ trials). Bottom, mean fluorescence changes across all trials ($n = 120$ trials of 2 rats). **d**, Top, schematic of dual-color photometry in the NAc of wild-type rats coexpressing RdLight1 injected in the NAc and axon-GCaMP6f injected in mPFC. Bottom, representative micrograph showing RdLight1 in red and axon-GCaMP6f in green ($n = 2$ rats). Scale bar, 50 µm. **e**,**f**, Data are as described in **b** and **c**, except axon-GCaMP6f was measured instead of iGluSnFR.

be combined with scanned line angular projection microscopy for ultrafast imaging of DA release[28–30].

RdLight1 is a red genetically encoded membrane-integrated intensiometric sensor with a positive response and robust photostability and SNR in vivo. While existing red calcium sensors can be easily used for imaging of local neuronal activity (at the level of neuronal somata), their susceptibility to photobleaching compared with green calcium sensors[18,31] can present challenges under specific imaging conditions. For example, when distal-neural-projection activity needs to be measured together with local DA release, multiplexed use of RdLight1 with a green calcium probe (for example, GCaMP6f) is a valuable option. Furthermore, a red-shifted spectrum enhances SNR, which is likely due to lower autofluorescence and increased imaging depth (Extended Data Fig. 10a).

How DA dynamics shape the activity of postsynaptic neurons is also a long-standing question[32]. Simultaneous monitoring of DA release (with RdLight) and calcium dynamics in D1+ neurons (with GCaMP6f) may spur broader application of multicolor photometry in behaving animals. In brain slices, DA increases excitability of D1+ striatal neurons[33]. Our working hypothesis is that the cue-evoked DA release makes D1+ neurons more responsive to excitatory glutamatergic inputs—particularly from sources such as the medial frontal cortex[34]—and that these are ultimately responsible for driving the large increase in D1+ GCaMP signal we observed as the rats behaviorally responded to the reward cue. However, dual-color monitoring of RdLight1 and iGluSnFR revealed that reward-predictive cues provoke a marked decrease, rather than an increase, in glutamate release. We had expected to observe a fast glutamate increase, in part because such cues evoke rapid increases in spiking in many neurons within brain areas that provide glutamatergic inputs to NAc, including medial frontal cortex[35] and basolateral amygdala[36]. For this and other reasons, models of DA–glutamate interactions typically assume that salient cues evoke a strong glutamate increase in NAc, that would spill out of synaptic clefts[37]. Given the very limited spatial resolution of fiber photometry, our observation of a cue-evoked decrease in bulk extracellular glutamate suggests that the specific NAc glutamate synapses involved in evoking motivated behavior are relatively sparse with little spillover. This is in marked contrast to volume-conducted DA signals[38]. The rapid, widespread DA increase would presumably act on D2 receptors over a large proportion of glutamatergic synapses to produce the (slightly delayed) glutamate decrease we observed. The lack of a rapid cue-evoked glutamate increase is also noteworthy since many DA cells coexpress glutamate as a neurotransmitter[24]. This may simply reflect our fiber placement in the NAc core rather than the medial NAc shell, which receives more joint DA and glutamate input[39]. Additional possibilities worth exploring are that the neurons coexpressing DA and glutamate are preferentially unresponsive to cues, or that glutamate is not released during burst firing of DA neurons. Regardless, the ability to monitor DA and glutamate dynamics simultaneously in real-time—rather than on the multiple-minutes time scale of microdialysis—will be useful for investigating the interactions between these neurotransmitters, both in normal behaviors and in models of human disorders, including drug addiction[40].

End users should first optimize the expression level of the sensor to be matched with imaging conditions in order to maximize SNR. Virus-mediated gene-expression level varies depending on promoter, serotype and other conditions[41]. As dLight1-type sensors are based on inert GPCRs, their high affinity to endogenous ligands may be a double-edged sword. While one can be confident that the affinity is within the physiological range, overexpression of the sensor may buffer DA availability at endogenous DA receptors. In our specific experimental conditions, we demonstrated that dLight1-type sensors do not engage G-protein or beta-arrestin signaling in vitro. In addition, overexpression of RdLight1 and dLight1 does not appreciably affect NAc function in vivo. Nevertheless, careful evaluation of the sensor's effect on signaling cascades, circuit activity and behavior in other conditions and brain regions is needed for end users.

Since many new GPCR-based sensors are continuously being introduced, such as GRAB-DA, GRAB-NE and GACh[2,42,43], RdLight1 opens doors to study neurotransmitter release and modulatory effects on neural circuits, and serves as an example for how to expand the color spectrum of GPCR-based sensors. Future engineering efforts are expected to improve sensor brightness and dynamic range (for example, to assist two-photon imaging) and to further stretch the color palette (for example, to far red)[44,45], allowing even more signals to be monitored simultaneously.

Online content

Any methods, additional references, Nature Research reporting summaries, source data, extended data, supplementary information, acknowledgements, peer review information; details of author contributions and competing interests; and statements of data and code availability are available at https://doi.org/10.1038/s41592-020-0936-3.

Received: 2 December 2019; Accepted: 23 July 2020;
Published online: 07 September 2020

References

1. Patriarchi, T. et al. Ultrafast neuronal imaging of dopamine dynamics with designed genetically encoded sensors. *Science* **360**, eaat4422 (2018).
2. Sun, F. et al. A genetically encoded fluorescent sensor enables rapid and specific detection of dopamine in flies, fish, and mice. *Cell* **174**, 481–496.e19 (2018).
3. de Jong, J. W. et al. A neural circuit mechanism for encoding aversive stimuli in the mesolimbic dopamine system. *Neuron* **101**, 133–151.e7 (2019).
4. Mohebi, A. et al. Dissociable dopamine dynamics for learning and motivation. *Nature* **570**, 65–70 (2019).
5. Zhao, Y. et al. An expanded palette of genetically encoded Ca^{2+} indicators. *Science* **333**, 1888–1891 (2011).
6. Dana, H. et al. Sensitive red protein calcium indicators for imaging neural activity. *Elife* **5**, e12727 (2016).
7. Kruss, S. et al. High-resolution imaging of cellular dopamine efflux using a fluorescent nanosensor array. *Proc. Natl Acad. Sci. USA* **114**, 1789–1794 (2017).
8. Beyene, A. G. et al. Imaging striatal dopamine release using a nongenetically encoded near infrared fluorescent catecholamine nanosensor. *Sci. Adv.* **5**, eaaw3108 (2019).
9. Wachter, R. M., Elsliger, M. A., Kallio, K., Hanson, G. T. & Remington, S. J. Structural basis of spectral shifts in the yellow-emission variants of green fluorescent protein. *Structure* **6**, 1267–1277 (1998).
10. Orm, M. et al. Crystal structure of the *Aequorea victoria* green fluorescent protein. *Science* **273**, 1392–1395 (1996).
11. Nagai, T. et al. A variant of yellow fluorescent protein with fast and efficient maturation for cell-biological applications. *Nat. Biotechnol.* **20**, 87–90 (2002).
12. Ade, K., Wan, Y., Chen, M., Gloss, B. & Calakos, N. An improved BAC transgenic fluorescent reporter line for sensitive and specific identification of striatonigral medium spiny neurons. *Front. Syst. Neurosci.* **5**, 32 (2011).
13. Eichel, K. et al. Catalytic activation of β-arrestin by GPCRs. *Nature* **557**, 381–386 (2018).
14. Kebabian, J. W. et al. A-77636: a potent and selective dopamine D1 receptor agonist with antiparkinsonian activity in marmosets. *Eur. J. Pharmacol.* **229**, 203–209 (1992).
15. Oe, Y. et al. Distinct temporal integration of noradrenaline signaling by astrocytic second messengers during vigilance. *Nat. Commun.* **11**, 471 (2020).
16. Marvin, J. S. et al. An optimized fluorescent probe for visualizing glutamate neurotransmission. *Nat Methods* **10**, 162–170 (2013).
17. Villette, V. et al. Ultrafast two-photon imaging of a high-gain voltage indicator in awake behaving mice. *Cell* **179**, 1590–1608.e23 (2019).
18. Chen, T.-W. et al. Ultrasensitive fluorescent proteins for imaging neuronal activity. *Nature* **499**, 295–300 (2013).
19. Witten, I. B. et al. Recombinase-driver rat lines: tools, techniques, and optogenetic application to dopamine-mediated reinforcement. *Neuron* **72**, 721–733 (2011).
20. Hamid, A. A. et al. Mesolimbic dopamine signals the value of work. *Nat. Neurosci.* **19**, 117–126 (2016).
21. Stujenske, J. M., Spellman, T. & Gordon, J. A. Modeling the spatiotemporal dynamics of light and heat propagation for in vivo optogenetics. *Cell Rep.* **12**, 525–534 (2015).
22. Broussard, G. J. et al. In vivo measurement of afferent activity with axon-specific calcium imaging. *Nat. Neurosci.* **21**, 1272–1280 (2018).
23. Pettibone, J. R. et al. Knock-in rat lines with Cre recombinase at the dopamine D1 and adenosine 2a receptor loci. *Eneuro* https://doi.org/10.1523/ENEURO.0163-19.2019 (2019).
24. Hnasko, T. S. et al. Vesicular glutamate transport promotes dopamine storage and glutamate corelease in vivo. *Neuron* **65**, 643–656 (2010).
25. Schultz, W. Dopamine reward prediction-error signalling: a two-component response. *Nat. Rev. Neurosci.* **17**, 183–195 (2016).
26. Kalivas, P. W. & Duffy, P. Dopamine regulation of extracellular glutamate in the nucleus accumbens. *Brain Res.* **761**, 173–177 (1997).
27. Nicola, S. M., Taha, S. A., Kim, S. W. & Fields, H. L. Nucleus accumbens dopamine release is necessary and sufficient to promote the behavioral response to reward-predictive cues. *Neuroscience* **135**, 1025–1033 (2005).

28. Marvin, J. S. et al. Stability, affinity, and chromatic variants of the glutamate sensor iGluSnFR. *Nat. Methods* **15**, 936–939 (2018).
29. Kazemipour, A. et al. Kilohertz frame-rate two-photon tomography. *Nat. Methods* **16**, 778–786 (2019).
30. Liu, R., Li, Z., Marvin, J. S. & Kleinfeld, D. Direct wavefront sensing enables functional imaging of infragranular axons and spines. *Nat. Methods* **16**, 615–618 (2019).
31. Dana, H. et al. High-performance calcium sensors for imaging activity in neuronal populations and microcompartments. *Nat. Methods* **16**, 649–657 (2019).
32. Gerfen, C. R. & Surmeier, D. J. Modulation of striatal projection systems by dopamine. *Ann. Rev. Neurosci.* **34**, 441–466 (2011).
33. Planert, H., Berger, T. K. & Silberberg, G. Membrane properties of striatal direct and indirect pathway neurons in mouse and rat slices and their modulation by dopamine. *PLoS ONE* **8**, e57054 (2013).
34. Ishikawa, A., Ambroggi, F., Nicola, S. M. & Fields, H. L. Dorsomedial prefrontal cortex contribution to behavioral and nucleus accumbens neuronal responses to incentive cues. *J. Neurosci.* **28**, 5088–5098 (2008).
35. Burgos-Robles, A., Bravo-Rivera, H. & Quirk, G. J. Prelimbic and infralimbic neurons signal distinct aspects of appetitive instrumental behavior. *PLoS ONE* **8**, e57575 (2013).
36. Ambroggi, F., Ishikawa, A., Fields, H. L. & Nicola, S. M. Basolateral amygdala neurons facilitate reward-seeking behavior by exciting nucleus accumbens neurons. *Neuron* **59**, 648–661 (2008).
37. Bamford, N. S., Wightman, R. M. & Sulzer, D. Dopamine's effects on corticostriatal synapses during reward-based behaviors. *Neuron* **97**, 494–510 (2018).
38. Rice, M. E. & Cragg, S. J. Dopamine spillover after quantal release: rethinking dopamine transmission in the nigrostriatal pathway. *Brain Res. Rev.* **58**, 303–313 (2008).
39. Hnasko, T. S., Hjelmstad, G. O., Fields, H. L. & Edwards, R. H. Ventral tegmental area glutamate neurons: electrophysiological properties and projections. *J. Neurosci.* **32**, 15076–15085 (2012).
40. McFarland, K. & Kalivas, P. W. The circuitry mediating cocaine-induced reinstatement of drug-seeking behavior. *J. Neurosci.* **21**, 8655–8663 (2001).
41. Hioki, H. et al. Efficient gene transduction of neurons by lentivirus with enhanced neuron-specific promoters. *Gene Ther.* **14**, 872–882 (2007).
42. Feng, J. et al. A genetically encoded fluorescent sensor for rapid and specific in vivo detection of norepinephrine. *Neuron* **102**, 745–761.e8 (2019).
43. Jing, M. et al. A genetically encoded fluorescent acetylcholine indicator for in vitro and in vivo studies. *Nat. Biotechnol.* **36**, 726–737 (2018).
44. Qian, Y. et al. A genetically encoded near-infrared fluorescent calcium ion indicator. *Nat. Methods* **16**, 171–174 (2019).
45. Ravotto, L., Duffet, L., Zhou, X., Weber, B. & Patriarchi, T. A bright and colorful future for G-protein coupled receptor sensors. *Front. Cell. Neurosci.* **14**, 67 (2020).
46. Ke, M.-T., Fujimoto, S. & Imai, T. SeeDB: a simple and morphology-preserving optical clearing agent for neuronal circuit reconstruction. *Nat. Neurosci.* **16**, 1154–1161 (2013).

Methods

Molecular cloning. The red DA sensor library was generated using circular polymerase extension cloning (CPEC)[47]. pCMV.dLight1.3b was used as the destination vector, while the red fluorescent protein insert, containing circularly permuted mApple and original linker sequences (Extended Data Fig. 1), was PCR-amplified from jRGECO1a. To generate sensor libraries, the two-amino-acid-long linker regions on each side of cpmApple were then mutagenized with primers containing random codon sequences. BamHI and HindIII sites were introduced via PCR for final subcloning onto pAAV.hSynapsin1 and pAAV.CAG viral vectors. Single colonies were manually picked and grown overnight as described in ref. [48]. All sensor sequences generated in this study are listed in the Supplementary Note.

Structural modeling and sequence alignments. Active conformations of the sensors were predicted with the rosetta_cm protocol of rosetta 3 (version 2015.31)[49]. The primary sequences of YdLight1 and RdLight1 were threaded with partial thread routine onto template PDB structures of active β_2AR[50] (ID: 3P0G) and Ca^{2+}-bound state of GCaMP3[51] (ID: 4IK3). The threaded structures were then hybridized together with the rosetta_cm protocol for membrane protein[52]. A total of 10,595 and 9,828 PDB structures were generated by rosetta_script routine for YdLight and RdLight1, respectively. Structures with lowest total scores were considered the final models.

Cell culture, imaging and quantification. HEK293T cells (ATCC no. 1573) and U2OS cells (ATCC no. HTB-96) were cultured and transfected as in ref. [1]. Primary hippocampal and striatal neurons were freshly isolated and cultured as previously described[53,54]. Hippocampal neurons were virally transduced using AAVs (1×10^9 viral genomes per ml) at DIV5 2 weeks prior to imaging. Striatal neurons were transfected via electroporation (Rat Neuron Nucleofector Kit; Lonza) per the manufacturer's instructions. Immediately before imaging, cells were washed with HBSS (Life Technologies) supplemented with Ca^{2+} (2 mM) and Mg^{2+} (1 mM). Cell imaging was performed using a ×40 oil-based objective on an inverted Zeiss Observer LSN710 confocal microscope. The different color variants of the dopamine sensor were imaged using laser lines with the following wavelengths: 488 nm (dLight1.3b), 514 nm (YdLight1), 561 nm (RdLight1). For testing sensor responses, all neurotransmitters and drugs were directly applied to the bath during the imaging session. The one-photon emission spectrum for the sensors was determined using the lambda-scan function of the confocal microscope and the following laser lines: 488 nm for dLight1.3b and YdLight1, 561 nm for RdLight1. Surface labeling using anti-Flag antibody was achieved as described previously[55]. For selection of regions of interest, masks were generated on individual cell membranes using the threshold function in Fiji (ImageJ). For titration curves, apparent K_d values were obtained by fitting the data with a one-site-specific binding function on GraphPad Prism 6. We calculated spatial movies and images of $\Delta F/F$ in response to an applied ligand as $(F(t) - F_0) / F_0$, with $F(t)$ being the pixel-wise fluorescence value at each time, t, and the mean fluorescence in time points prior to ligand application being F_0. To avoid the possibility of infinite pixel values, we added a small offset to each pixel in F_0. On the basis of the $\Delta F/F$ maps, we calculated a corresponding SNR map as $\Delta F/F \times \sqrt{F_0}$. Heatmaps were generated using a custom-made MATLAB script.

When perfusion was performed, a ×20 objective was used. Imaging setting was kept constant across all the samples. Ligands (DA or NE) were diluted to 1 µM in HBSS with 2 mM $CaCl_2$ and 1 mM $MgCl_2$ (HBSSCaMg). Perfusion during imaging was done on RC-48LP low-profile open bath chambers (Warner Instruments); 5 ml of HBSSCaMg was used to flow through before and after 5 ml 1 µM ligands in HBSSCaMg.

For FACS analysis, the cells were deattached and basal fluorescence intensity were measured on BD FACScan cytometer. Both populations of cells transfected with either RdLight1 or nLight1.3 were excited with a 488-nm laser; the green channel emission filter was a 530/30 bandpass filter, transfected with either RdLight1 or nLight1.3and red channel was a 585/42 bandpass filter. Data were analyzed with flowCore package in Bioconductor[56].

Internalization assay with flow cytometry. At 24 h following transfection, cells were replated onto 6-well dishes. The following day, surface levels of receptors were assayed by addition of Alexa-647-conjugated M1 antibody (Sigma) for 45 min, as described previously[55]. Fluorescence-intensity profiles of cell populations (>5,000 cells) were measured using a FACS-Calibur instrument (BD Biosciences). Each condition was performed in duplicate. Internalization was calculated by measuring the fraction of surface fluorescence remaining after 30 min of 1 µM SKF81297 (Tocris) and divided by the non-treated condition.

Luminescence and fluorescence-based cAMP assays. Luminescence experiments were conducted as previously described[55]. Briefly, cells were transfected with the cyclic-permuted luciferase pGLOSensor-20F plasmid (Promega) 34 h before the experiment, and then were treated with luciferin (GoldBio) in phenol red and serum-free DMEM for 1 h in a 24-well dish. The indicated concentrations of SKF81297 (Tocris) were added, and luminescence values were measured at peak using a plate luminometer at 37 °C. Then, 10 µM forskolin (Sigma) was added and the peak luminescence value was measured to normalize the SKF81297 response across wells. Fluorescence measurements of cAMP accumulation in cultured striatal neurons were performed using a green genetically encoded cAMP sensor expressed by a CAG-promoter-driven baculovirus vector (Green Up cADDis, Montana Molecular)[57], and coexpression of RdLight1 was achieved by coinfection with AAV. Cells were imaged using an inverted spinning disk confocal microscope and ×60 NA-1.4 oil-immersion objective. Laser illumination at 488 nm was used to excite the cAMP sensor, 561-nm illumination was used to excite intrinsic RdLight1 fluorescence and 561-nm illumination was used to excite the Alexa-647-conjugated anti-Flag monoclonal antibody detecting surface expression of RdLight1. Kinetics of the cAMP response were determined by sequential imaging at 37 °C, with a SKF81297 bath applied at 1 µM, and with 10 µM forskolin added at the end of the acquisition series to normalize responses across neurons.

Total internal reflection fluorescence microscopy live imaging. Live-cell total internal reflection fluorescence microscopy was conducted with a Nikon Ti-E inverted microscope at 37 °C in a controlled humidity and CO_2-controlled chamber, as described previously[55]. D1-specific agonist SKF81297 (Tocris) was added at 1 µM, while D1 antagonist SCH-23390 (Tocris) was added at 10 µM.

AAV viral production. All RdLight1 AAV constructs were cloned in the laboratory. RdLight1 and axon-GCaMP6f viruses were produced by the UC Davis Vision Center Vector Design and Packaging Core facility. The viral titers of the viruses used in this study were: AAV9.*CAG*.RdLight1, ~1×10^{12} genome counts (GC) ml^{-1}; AAV9.*hSynapsin1*.RdLight1, ~1×10^{12} GC ml^{-1}; AAV1.*hSynapsin1*.GCaMP6s, ~1×10^{12} GC ml^{-1}; AAV9.*CAG*.Flex.GCaMP6f, ~1×10^{12} GC ml^{-1}; AAV5.*hSynapsin1*.iGluSnFR, ~2.9×10^{12} GC ml^{-1}; AAV1.*hSynapsin1*.axon-GCaMP6f, ~1×10^{12} GC ml^{-1}.

Animals. Animal studies were conducted in compliance with the Guide for the Care and Use of Laboratory Animals of the National Institutes of Health and approved by the Institutional Animal Care and Use Committee (IACUC) at the University of California, Davis, or the relevant institutional regulatory body.

Viral injections. Injection procedures were essentially identical to those described in ref. [1], with a few exceptions. For DA, glutamate and calcium imaging in brain slices, male and female C57/Bl6 mice (8–12 weeks old) were used for intracerebral microinjections. Briefly, anesthetized mice were immobilized in a stereotaxic alignment system (Kopf Instruments). AAV9.*hSynapsin1*.RdLight1 alone or mixed at 1:1 ratio in combination with either AAV5.*hSynapsin1*.iGluSnFR or AAV9.*hSynapsin1*.GCaMP6s was injected undiluted at a total volume of 150 nl unilaterally into the dorsal striatum using the following coordinates from bregma (in mm): + 0.8 anteroposterior (AP) ± 1.5 mediolateral (ML), −3.2 dorsoventral (DV).

Slice preparation and ex vivo two-photon imaging. At 2–4 weeks after viral injection, mice were anesthetized with 2.5% avertin and decapitated. The heads were placed in high-sucrose artificial cerebrospinal fluid (aCSF) that contained (in mM) 73 NaCl, 2.5 KCl, 2 $MgCl_2$, 1.25 NaH_2PO_4, 25 $NaHCO_3$, 24 dextrose, 0.5 $CaCl_2$ and 75 sucrose, saturated with 95% O_2 and 5% CO_2. The brains were then removed from the skull and cut (400 µm) with a vibratome (V1200s, Leica) in ice-cold high-sucrose aCSF. Brain slices were incubated at 32 °C for 30 min in normal aCSF that contained (in mM) 128 NaCl, 2.5 KCl, 1 $MgCl_2$, 1.25 NaH_2PO_4, 25 $NaHCO_3$, 10 dextrose and 2 $CaCl_2$, 300 mOsm, saturated with 95% O_2 and 5% CO_2. After incubation, slices were placed in aCSF at room temperature for 30 min before imaging. Imaging was carried out in a two-photon microscope with a heated slice perfusion system, enabling recordings at 37 °C. Fluorescence of both green and red indicators was excited at 1020 nm with a Ti:sapphire laser (Ultra II, Coherent) that was focused by an Olympus ×40, 0.8-NA water immersion objective. Emitted light from the two indicators was separated using the following filter sets: 525/50 nm and 620/60 nm. Data were acquired and collected with ScanImage5 software. Electrical stimulation was performed by placing a metal bipolar electrode (PI2ST30.01A5, Microprobes for Life Science) within the slice approximately 50 µm away from the area of imaging. Different numbers of pulses of identical amplitude and duration (4 V, 0.5 ms each) were applied though a Grass SD9 stimulator. Triggers for imaging and electrical stimulation were controlled by Axon Digidata 1550B. Experiments were carried out with a scan rate of 198 (64×64 pixels) or 30 (512×512 pixels) Hz. The fluorescence over the entire field (7.5×7.5 µm for 198 Hz, 60×60 µm for 30 Hz) was measured for each frame and plotted against time. Drugs were dissolved as a stock solution either in DMSO or in aCSF, and diluted at least 1:10,000 prior to application in the perfusion system. Image analysis was performed with ImageJ, and curve fits and data analyses were calculated using OriginPro 8.0 and SigmaPlot 12.0. Electric stimulation in different situations (without or with drug) was repeatedly applied 3 times (20-s interval) on each slice. Overall fluorescence of the whole frame was analyzed and averaged to improve SNR. Gray trials in Fig. 2 show the average results from all slices. Tau_{on} was calculated by fitting the fluorescence rise with a linear regression, and Tau_{off} was calculated by fitting the fluorescence decay with a single exponential curve. The inset shows zoomed-in view of the fluorescence peak.

Two-photon bleaching measurements. Two-photon bleaching measurements of RdLight were acquired from acute brain slices. Laser excitation was at 1020 nm and focused by an Olympus ×40, 0.8-NA water immersion objective. Emitted fluorescence photons were separated by a 620/60-nm filter. The scan area was 60 µm × 60 µm, and the scan rate was 30 frames per s. Light intensity was kept at 8.7 mW across measurements. Burst electrical stimulation was performed with a metal bipolar electrode (PI2ST30.01A5, Microprobes for Life Science) every 100 s. Amplitude of the pulses was 4 V, width was 0.3 ms and a total number of 40 pulses was applied at a frequency of 80 Hz.

Histology and confocal imaging. Mice were deeply anesthetized with 2.5% avertin and transcardially perfused with 10 ml 1× DPBS (Gibco), followed by 50 ml 4% paraformaldehyde in DPBS. After perfusion, the brains were removed and postfixed overnight at 4°C. The brains were embedded in 5% sucrose in DPBS overnight at 4°C, and then embedded in 15% sucrose in DPBS for 48 h. Fixed brains were cut into 30-µm-thick coronal sections with a vibratome (Leica CM 3050 S). Sections were coverslipped with mounting medium (ProLong Glass Antifade Mountant, Thermo Fisher Scientific). Confocal images (LSM 710, Zeiss) were collected using a ×40, 1.3-NA oil objective. Emitted light was separated using the following filter sets: 488 nm and 561 nm. Data were acquired with Zen software and analyzed with ImageJ.

In vivo fiber photometry. We used a viral approach to express different genetically encoded indicators and actuators in the brain. We injected 1 µl of AAV1.*hSynapsin1*.FLEX.axon-GCaMP6f or AAV5.*EF1a*.FLEX.ChR2.eYFP slowly into the lateral VTA (AP: −5.7, ML: 0.9, DV: −7.5 mm) and AAV9.*CAG*.RdLight1 or AAV9.*hSynapsin1*.iGluSnFR into the ventral striatum (AP: 1.7, ML: 1.7, DV: −7.0 mm). During the same surgery, a 400-µm core optical fiber was implanted 200 µm above the injection site and anchored to skull using dental cement. For GCaMP6f, we used a 470 nm blue excitation LED (Thorlabs) and 405 nm violet for isosbestic control, modulated at different frequencies (211 Hz and 531 Hz). We used a 565-nm red-shifted LED to excite RdLight1 at 340 Hz frequency. All three excitation signals were passed through a six-port filter cube (Doric), and emission signals were amplified using a picowatt amplifier (Newport, model 2151) and saved on the disk using a Labview-based data-acquisition system. Output of the amplifiers were demodulated offline to separate the indicator and control responses.

All photometry recordings were done in operant training chambers (Med Associates; 25 cm × 30 cm), with five nosepoke ports and a food-retrieval cup with the houselight on. Rats were mildly food deprived (receiving 15 g of standard laboratory rat chow daily) and received between 5 and 8 training sessions before the experiment. Each session consisted of 60 trials each of unpredictable rewards; cues predicting reward with 75% probability; and cues predicting reward with 25% probability, randomly interleaved, with random inter-trial intervals (15–30 s, uniform distribution). Cues were trains of auditory tone pips (2 KHz or 9 KHz, 100 ms on, 50 ms off), associated with 75% or 25% chance of reward delivery 2.8 s after cue onset, as in ref. [4].

Statistics and reproductivity. All statistical analyses were performed in MATLAB (MathWorks R2017a), Igor Pro (WaveMetrics) or Prism (GraphPad). For determining statistical significance, we used either parametric (paired *t*-test, one-way analysis of variance) or non-parametric tests (Kolmogorov–Smirnov test). All tests were two-tailed. Error bars are s.e.m. or s.d., as indicated in the figure legends and main text. No statistical methods were used to predetermine sample size. When representative images and micrographs or single-trial fluorescence responses are shown, experiments were performed either at least three times or across many trials (trial numbers are stated in the figure legends), unless otherwise noted.

Reporting Summary. Further information on research design is available in the Nature Research Reporting Summary linked to this article.

Data availability

All DNA plasmids and viruses used in this study have been deposited in NCBI (accession numbers MK751449 and MK751450) and ADDGENE, and can be obtained either from the Tian laboratory at UC Davis, Addgene or the Canadian neurophotonics platform viral (https://tools.neurophotonics.ca/) core under a material-transfer agreement. All source data present in this manuscript are available from https://github.com/lintianlab/RdLight1. Source data are provided with this paper.

Code availability

Custom MATLAB code is available via https://github.com/lintianlab/RdLight1.

References

47. Quan, J. & Tian, J. Circular polymerase extension cloning. *Methods Mol. Biol.* **1116**, 103–117 (2014).
48. Tian, L. et al. Imaging neural activity in worms, flies and mice with improved GCaMP calcium indicators. *Nat. Methods* **6**, 875–881 (2009).
49. Song, Y. et al. High-resolution comparative modeling with RosettaCM. *Structure* **21**, 1735–1742 (2013).
50. Rasmussen, S. G. F. et al. Structure of a nanobody-stabilized active state of the β2 adrenoceptor. *Nature* **469**, 175–180 (2011).
51. Chen, Y. et al. Structural insight into enhanced calcium indicator GCaMP3 and GCaMPJ to promote further improvement. *Protein Cell* **4**, 299–309 (2013).
52. Bender, B. J. et al. Protocols for molecular modeling with Rosetta3 and RosettaScripts. *Biochemistry* **55**, 4748–4763 (2016).
53. Kotowski, S. J., Hopf, F. W., Seif, T., Bonci, A. & von Zastrow, M. Endocytosis promotes rapid dopaminergic signaling. *Neuron* **71**, 278–290 (2011).
54. Patriarchi, T. et al. Imaging neuromodulators with high spatiotemporal resolution using genetically encoded indicators. *Nat. Protoc.* **14**, 3471–3505 (2019).
55. Irannejad, R. et al. Conformational biosensors reveal GPCR signalling from endosomes. *Nature* **495**, 534–538 (2013).
56. Ellis, B. et. al. flowCore: basic structures for flow cytometry data. R package version 1.52.1. (2019).
57. Tewson, P. H., Martinka, S., Shaner, N. C., Hughes, T. E. & Quinn, A. M. New DAG and cAMP sensors optimized for live-cell assays in automated laboratories. *J. Biomol. Screen* **21**, 298–305 (2016).

Acknowledgements

This work was supported by NIH DP2MH107056 (L.T.); BRAIN Initiative awards U01NS090604, U01NS013522 (L.T. and M.V.Z), U01NS103571 (L.T) and U01NS094375 (J.B.); a Rita Allen Young Investigator Award (L.T.) and R01DA045783 (J.D.B.); the Olga Mayenfisch Foundation (T.P.); and the Novartis Foundation for medical-biological research (T.P.). We thank D. Jullie (UCSF) for advice and providing striatal neuronal culture. We thank J. Zhang and C.-H. Chen for advice on FACS experiments.

Author contributions

T.P., A. Mohebi, J.S., M.V.Z., J.D.B. and L.T. wrote the manuscript. T.P. developed the sensors and performed in vitro sensor characterization, in vitro multiplex imaging experiments and part of the viral injections for two-photon imaging in brain slices. J.S. performed part of the viral injections, tissue histology, electrophysiology and two-photon imaging and bleaching experiments. A. Mohebi performed in vivo photometry and optogenetic experiments. A. Marley and M.V.Z. performed TIRF microscopy, cAMP measurements and β-arrestin recruitment assays. R.L. generated the structural models of the sensors and performed FACS characterization of sensor coexpression. C.D. performed viral injections and characterization of the sensor's photoactivation properties. K.P. and B.W. participated in experimental planning for in vivo characterization. C.M.D. and G.O.M performed dissociated neuronal culture. All authors analyzed the data.

Competing interests

L.T. and G.O.M. are co-founders of Seven Biosciences.

Additional information

Extended data is available for this paper at https://doi.org/10.1038/s41592-020-0936-3.

Supplementary information is available for this paper at https://doi.org/10.1038/s41592-020-0936-3.

Correspondence and requests for materials should be addressed to M.v.Z., J.D.B. or L.T.

Peer review information Nina Vogt was the primary editor on this article and managed its editorial process and peer review in collaboration with the rest of the editorial team.

Reprints and permissions information is available at www.nature.com/reprints.

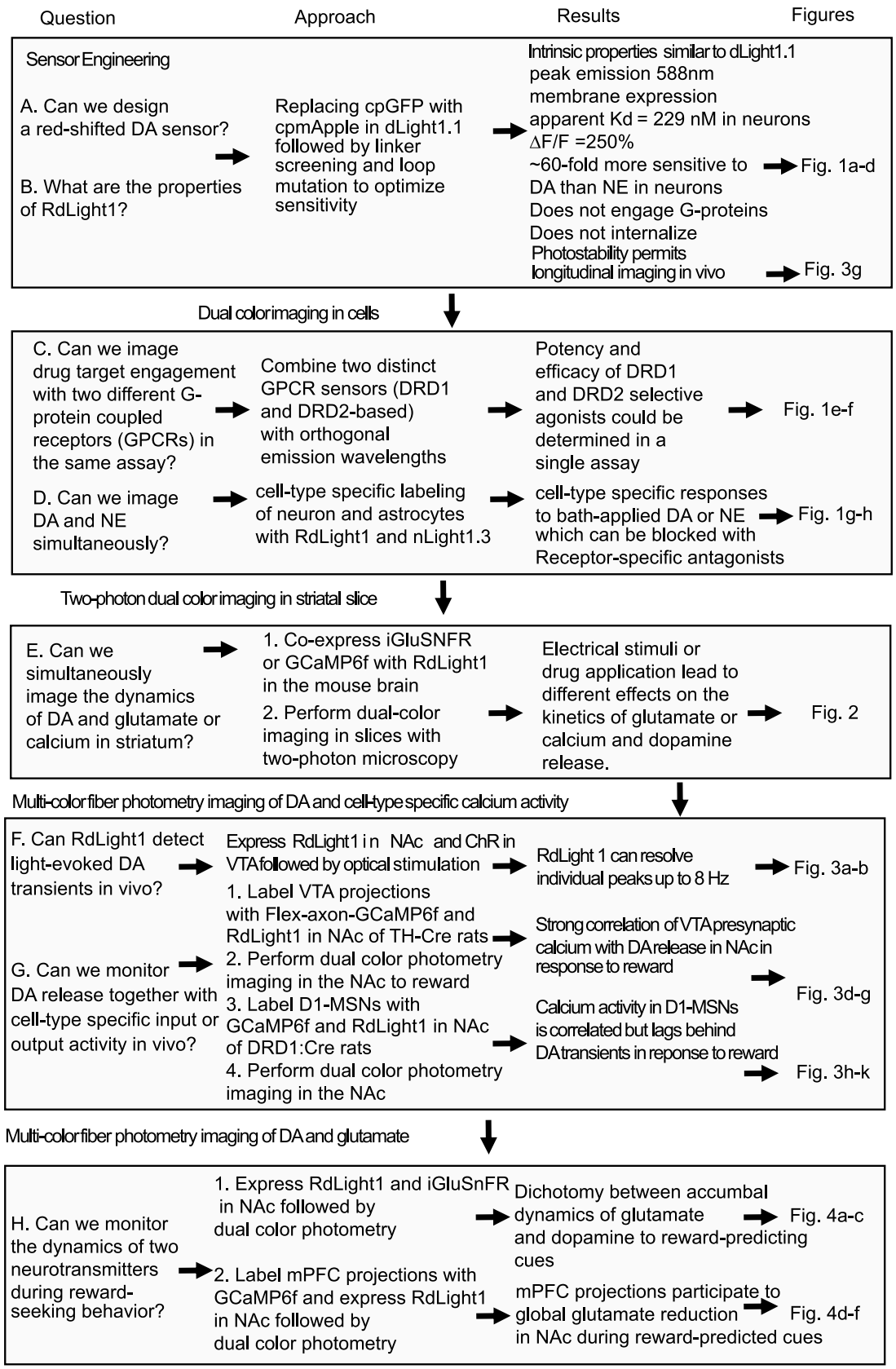

Extended Data Fig. 1 | Outline and summary of the experiments. Outline and summary.

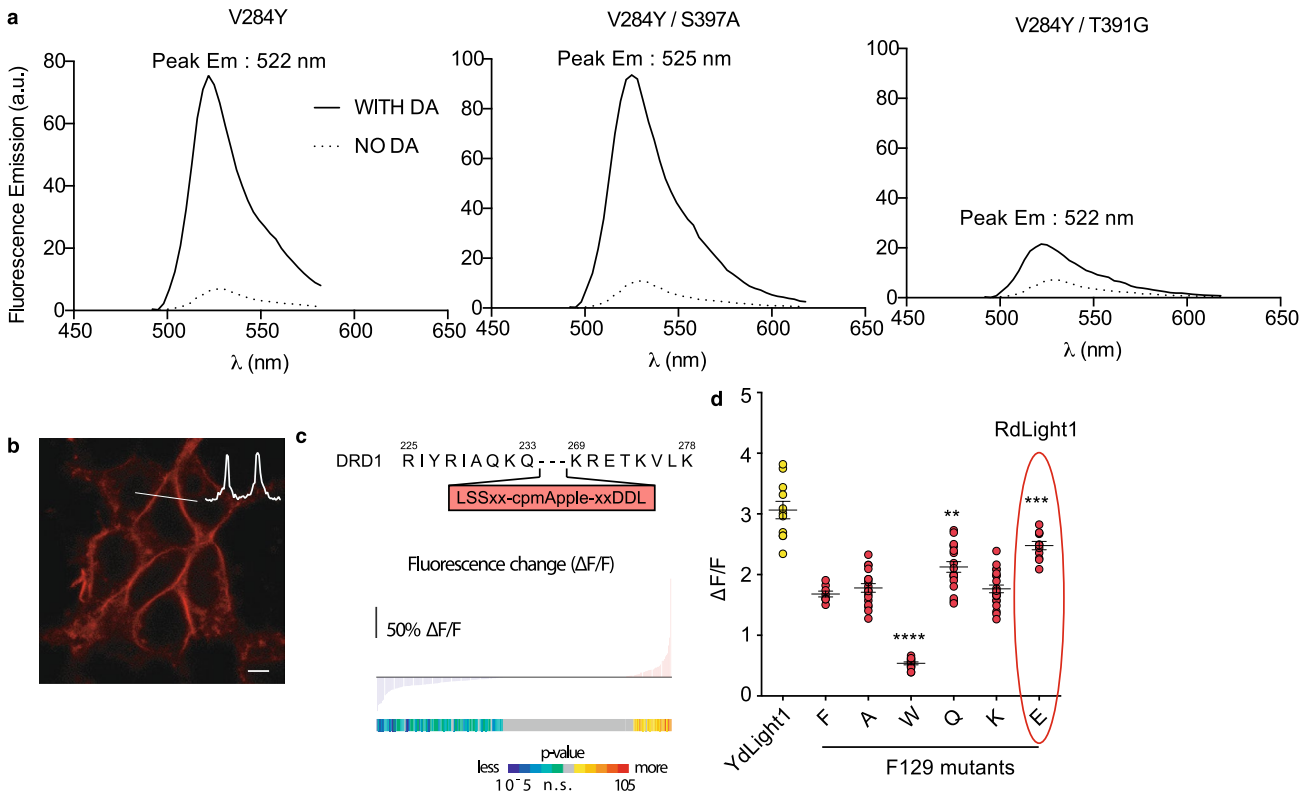

Extended Data Fig. 2 | Development of RdLight1. a, Fluorescence emission spectra of dLight1.3b variants carrying red-shifting mutations in their GFP component. Fluorescence emission was measured in the 450-650 nm wavelength range both in the absence of DA (dotted lines) and upon addition of 100 μM DA to the medium (continuous lines). n = 4 cells from 3 cultures. **b**, Representative image showing membrane expression profile of the initial variant of the red dopamine sensor, carrying the original amino acid linkers from JRGECO1a. The experiments were repeated at least twice with similar results. **c**, linker screening results from a library of 264 variants in which the two aminoacid pairs flanking cpmApple were randomized (as shown in inset). Red and blue vertical bars indicate fluorescence changes (ΔF/F) in response to 100 μM DA; significance values of ΔF/F are shown by colored bars and scale. n = 3 trials, two-tailed t test. **d**, optimization of the RdLight1 fluorescence response was achieved by selectively mutating residue F129 into a subset of amino acids. Fluorescence change (ΔF/F) was measured in HEK293 cells in response to bath-applied 100 μM DA. n = 4 cells from 2 cultures. **p<0.01, ****p<0.0001, two-tailed t test. The experiments were repeated at least twice with similar results. Data are shown as mean ± SEM.

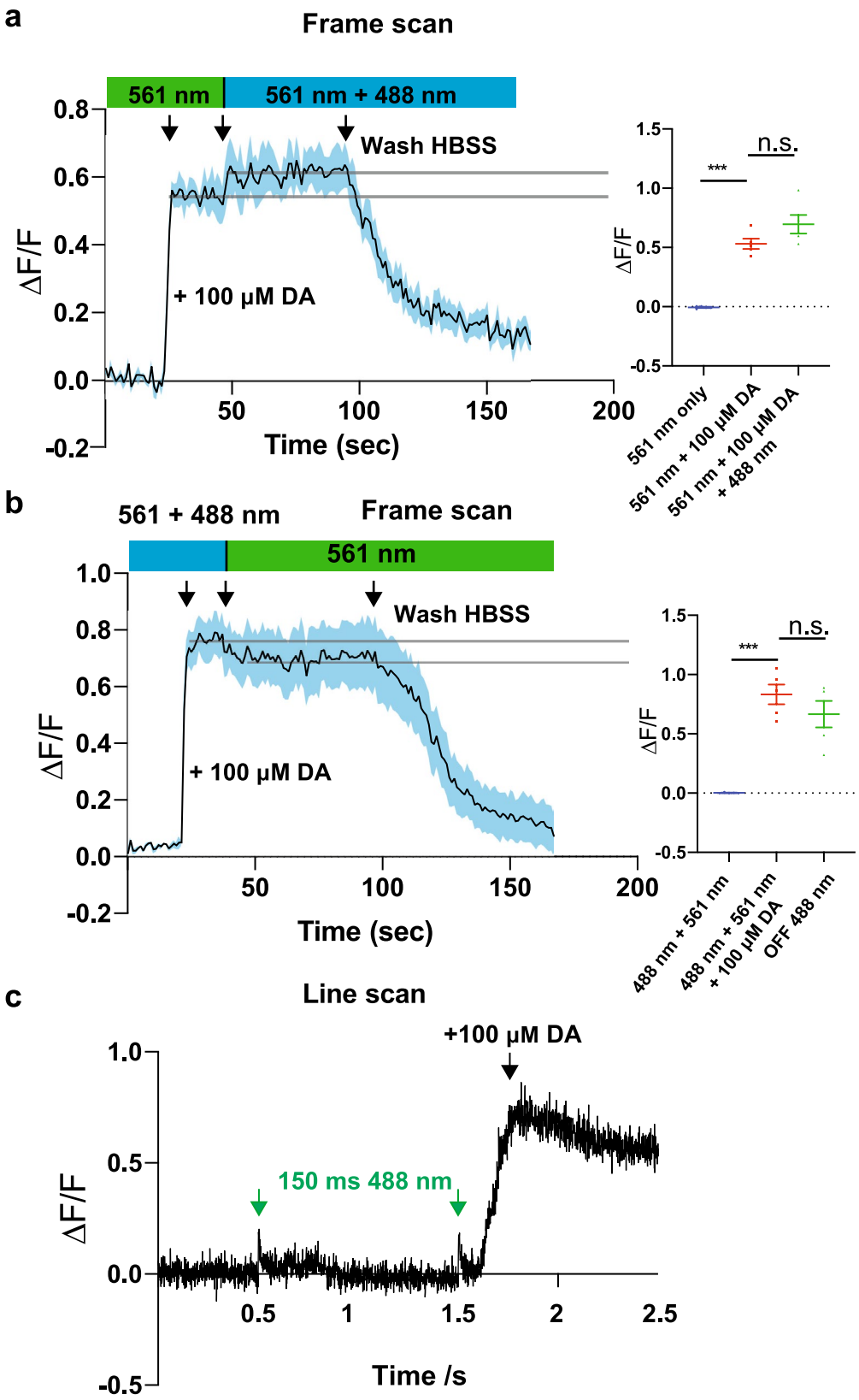

Extended Data Fig. 3 | Characterization of RdLight1 photoactivation by blue light. Confocal imaging of RdLight1 in transfected HEK293 cells. **a**, **b**, Frame scan imaging performed in the presence of both blue (488 nm) and green (561 nm) light after (a) or before (b) bath-application of DA. Blue light did not significantly increase the fluorescence response of RdLight1 to DA. Average ΔF/F=-0.006±0.003 (baseline), 0.53±0.03(DA), 0.69±0.06(DA+blue light, One-way Anova, ***P=0.0005, n.s P=0.1224, n=5 cells from two cultures (**a**). Average ΔF/=0.002±0.001 (baseline+blue light), 0.83±0.06(DA+blue light), 0.69±0.08(DA), One-way Anova, ***P=0.0007, n.s P=0.0678, n=5 cells from two cultures, mean±SEM (**b**). **c**, Representative line scan imaging at acquisition rate of 1000 Hz. Bursts of 488nm laser (150 ms duration at 1Hz) was applied followed by application of DA. Laser powers used were: 24779.4 W/cm^2 for 561nm laser, 16373.7 W/cm^2 for 488nm laser. Experiments were performed six times with similar results.

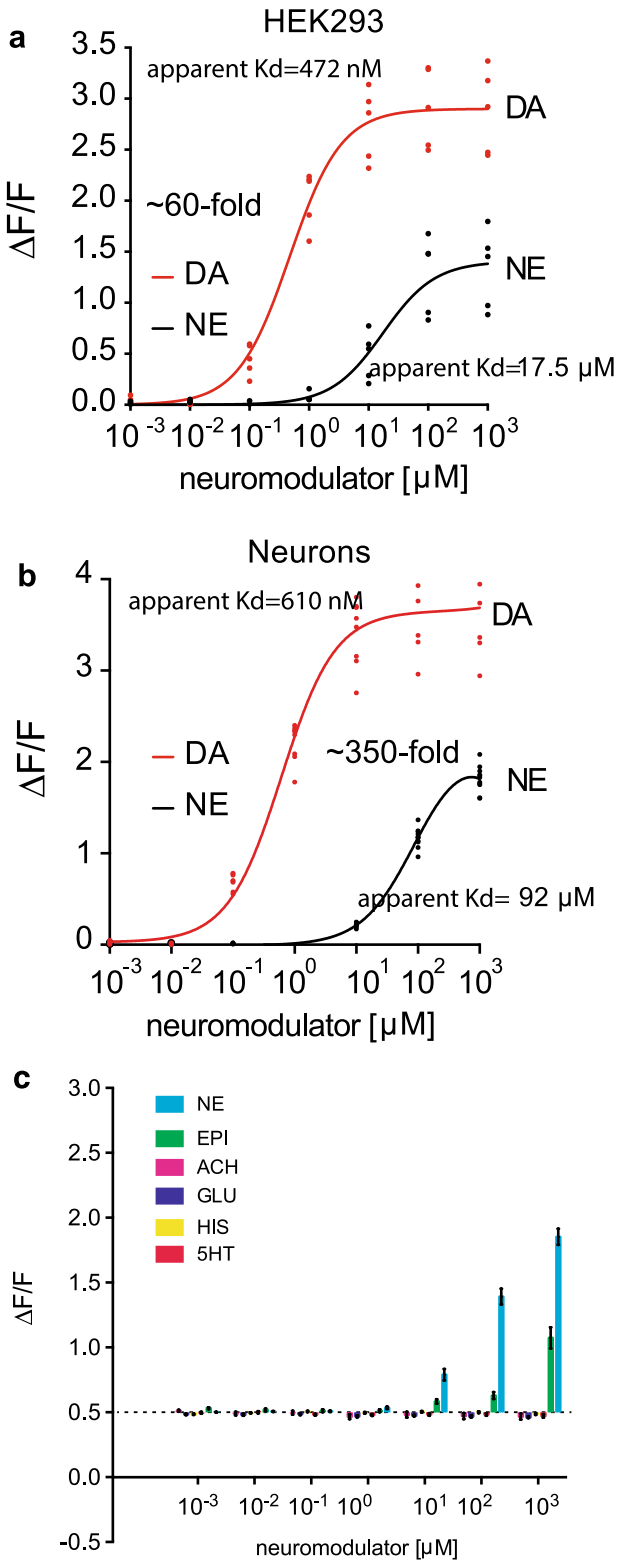

Extended Data Fig. 4 | Molecular specificity of RdLight1. a, **b**, Titration curves are shown for the response to DA or NE both in HEK293 cells and in cultured neurons. Data points were fit with a one-site specific binding curve to obtain EC_{50} values. Data are shown as mean ± SEM. n = 7 cells from 2 cultures for both HEK293 cells and neurons. The response of RdLight to NE at 1mM is significantly lower than that to DA ($P=4.8x10^{-8}$, paired t-test (two sided). **c**, The specificity of RdLight1 was tested by performing titrations of a panel of different neurotransmitters on the sensor expressed in HEK293 cells. Quantification of responses to each concentration of ligand are shown as mean ± SEM. n = 12 cells from 2 cultures. Neurotransmitters tested were: norepinephrine (NE), epinephrine (EPI), acetylcholine (ACH), glutamate (GLU), histamine (HIS), serotonin (5HT). The experiments were repeated at least twice with similar results.

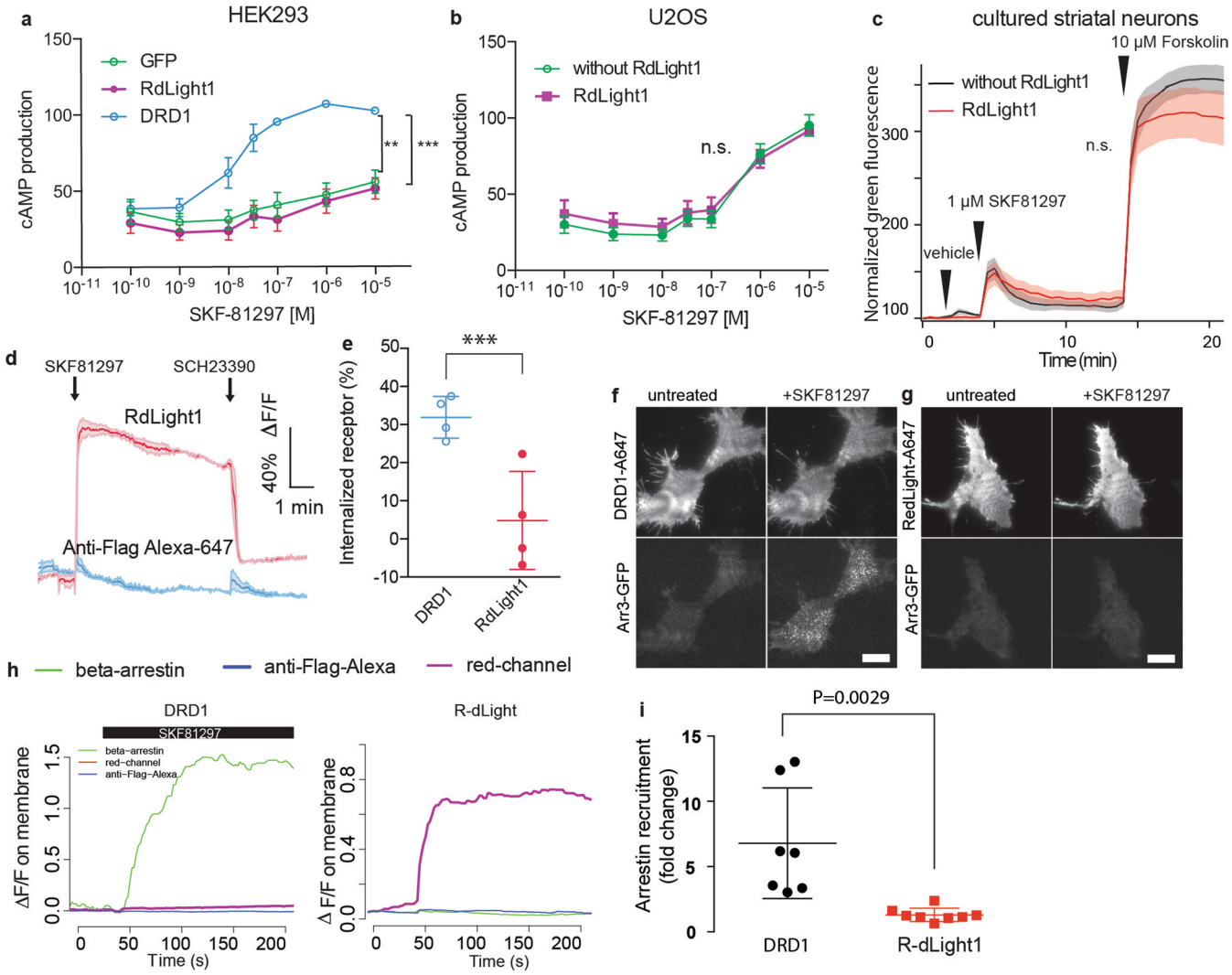

Extended Data Fig. 5 | Cellular signaling characterization of RdLight1. a, cAMP response curve to a titration of the D1 agonist SKF81297 in HEK293 cells transfected with RdLight1 compared to human D1-dopamine receptor (DRD1, positive control) or enhanced green fluorescence protein (GFP, negative control). No significant cAMP response was produced by RdLight1 (n=3 independent experiments, **p=0.0033, ***p=0.00053, one-way ANOVA, Dunnett's post-hoc test). **b**, cAMP response curves of a cell line endogenously expressing DRD1 (U2OS). Overexpression of RdLight1 did not alter the endogenous cAMP response to SKF81297 (n=3 independent experiments, p=0.944, two-way ANOVA). **c**, Expression of RdLight1 (red) in cultured primary striatal neurons did not affect cAMP responses to vehicle, SKF81297 or the adenylate cyclase activator Forskolin, compared to mock-transfected conditions (black), as measured by the green genetically encoded cAMP sensor cADDis (n=10 neurons from three cultures, P=0.744 (unpaired t-test, two-tailed). **d**, TIRF imaging of RdLight1 response (red) and of a static Alexa-647-conjugated anti-Flag antibody label to delineate sensor expression on cell surface (far-red channel). Quantification of RdLight1 response to a DRD1 agonist (SKF81297), which was immediately abolished by applying antagonist (SCH23390) (n=3 independent experiments). **e**, RdLight1 internalization is significantly reduced compared to wild type DRD1 as assayed via flow cytometry (% internalized receptor: RdLight1, 4.82 ± 6.42 %; DRD1, 31.9 ± 2.74 %, n=4 independent experiments, p=0.0006 (unpaired t-test, two-tailed). **f**, **g**, Representative TIRF microscopy images of HEK293 cells transfected with beta-arrestin-2 and DRD1 or RdLight1. DRD1 and RdLight1 were labeled with an Alexa-647 conjugated anti-flag antibody. Conditions before and after addition of DRD1 agonist SKF81297 are shown. Experiments were performed three times with similar results. **h**, **i**, Quantification of beta-arrestin-2 recruitment on the cell membrane from **f**, **g**. Under these conditions RdLight1 triggers significantly lower beta-arrestin-2 recruitment than DRD1. RdLight1, 6.8 ± 4.2 (n=8 cells); DRD1, 1.3 ± 0.5 (n=7 cells), P=0.0029 (unpaired t-test, two-tailed). All values shown are mean±SD.

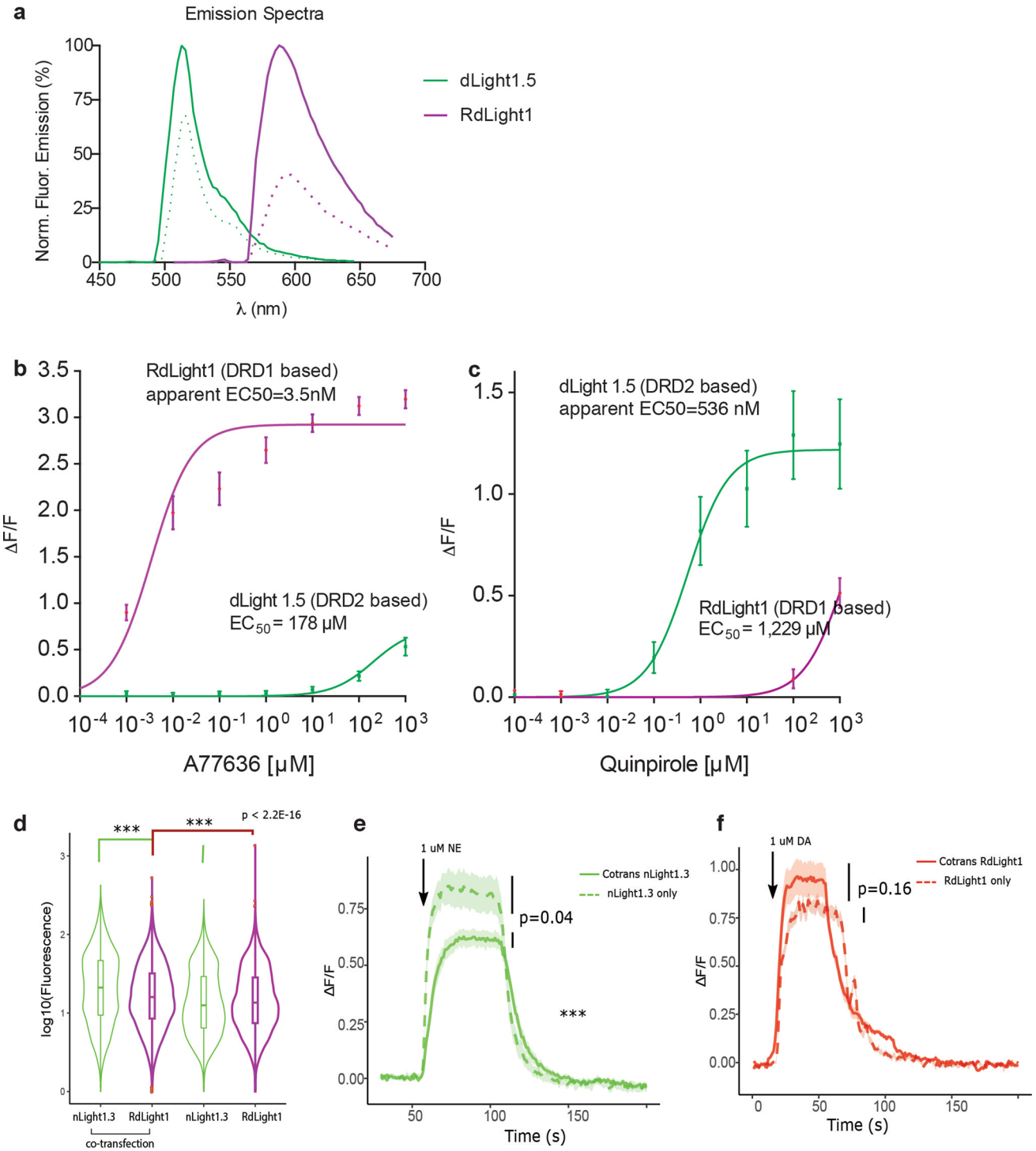

Extended Data Fig. 6 | Multiplex imaging of drug selectivity at two dopamine receptor subtypes and characterization of RdLight1 and nLight1.3 coexpression. a, Combined fluorescence emission spectra of DRD1-based (dLight1.5) and DRD1-based (RdLight1) sensors used for multiplex imaging experiments. Fluorescence emission was measured in the 450-700 nm wavelength range both in the absence of DA (dotted lines) and upon addition of 100 µM DA to the medium (continuous lines). n = 4 cells from 3 cultures. **b**, **c**, Dose-response curves were obtained by performing multiplex imaging during titrations of the DRD1-selective agonist A77636 or the DRD2-selective agonist Quinpirole on a coculture of two HEK293 cell populations expressing either RdLight1 (red) or dLight1.5 (green). Maximal fluorescence responses at each applied concentration were quantified and plotted. n = 6 cells from 3 cultures. Data are shown as mean ± SEM. **d**–**f**, Characterization of RdLight1 and nLight1.3 coexpression. **d**, Flow cytometry analysis of cells transfected with RdLight1 (n=13928 cells), nLight1.3(n=25798 cells), or both (n=33049 cells) showed that co-transfection significantly increased both basal green and basal red-fluorescence. Violin plots show the distribution of the log value of fluorescence, on top of the boxplot of the same data. P=2.2X10^{-16} Two-sided Student's t-test. **e**, **f**, In a perfusion experiment, confocal time-lapse imaging revealed that the response of nLight1.3 to NE when expressed alone (n=8) can be slightly decreased when cotransfected with RdLight1 (n=7 cells), which could possibly due to increased basal green fluorescence from RdLight1 co-transfection. A slight increase in the amplitude of response in RdLight1 was noticed when co-transfected (n=7 cells), but not significant. P=0.04 and 0.16, Two-sided Student's t-test for the value when NE or DA applied. Traces were plotted as mean +/- sem, with center line as mean value and shade the s.e.m.

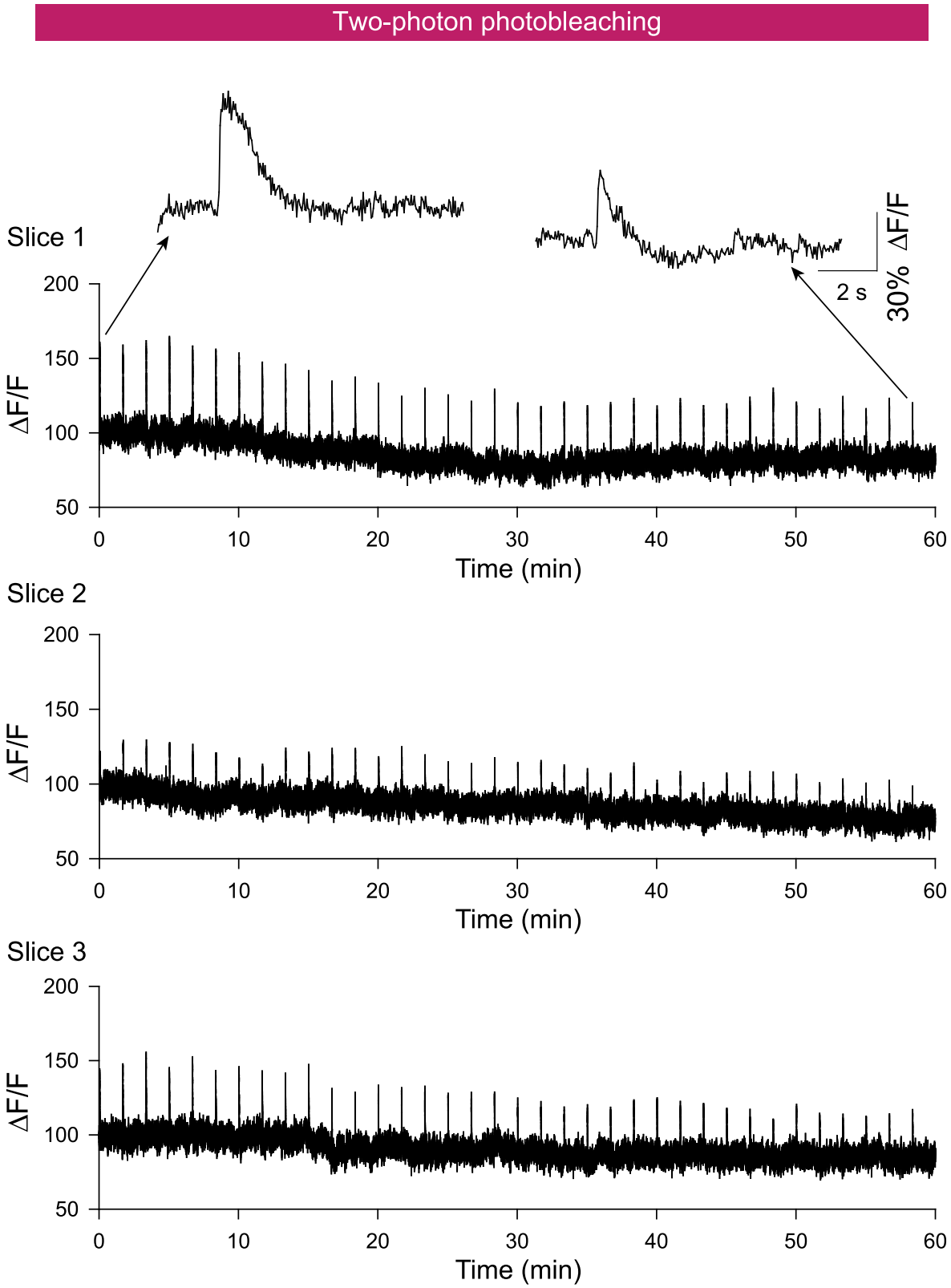

Extended Data Fig. 7 | Photobleaching of RdLight1 under two-photon illumination. Two-photon bleaching measurements of RdLight were acquired from acute brain slices. Fluorescence of RdLight was excited at 1020 nm with a Ti: sapphire laser (Ultra II, Coherent) that was focused by an Olympus 40×, 0.8NA water immersion objective. Emitted fluorescence photons were separated by a 620/60 nm filter. Scan area was 60 μm×60 μm, and the scan rate was 30 frames/s. Light intensity was kept at 8.7 mW across measurements. Burst electrical stimulation was performed with a metal bipolar electrode that has a tip spacing of 255 μm (PI2ST30.01A5, Microprobes for life science) every 100 s. Amplitude of the pulses was 4 V, width was 0.3 ms and a total number of 40 pulses was applied at a frequency of 80 Hz. As shown in the figure, photobleaching was continuously measured in a 1 h duration. Overall fluorescence in all the 3 tested slices declined about 17.2±3.1%, mean ± SEM. The experiments were repeated in 3 slices from two mice with similar results.

a

Symbol	Rat	Green indicator: injection	Red indicator: injection	Recording
⬣	TH-Cre	ChR2-eYFP: VTA	RdLight1: NAc	NAc
■	TH-Cre	axon-GCaMP6f: VTA	RdLight1: NAc	NAc
◆	D1-Cre	GCaMP6f: NAc	RdLight1: NAc	NAc
●	WT	iGluSnFR: NAc	RdLight1: NAc	NAc
★	WT	axon-GCaMP6f: mPFC	RdLight1: NAc	NAc

b

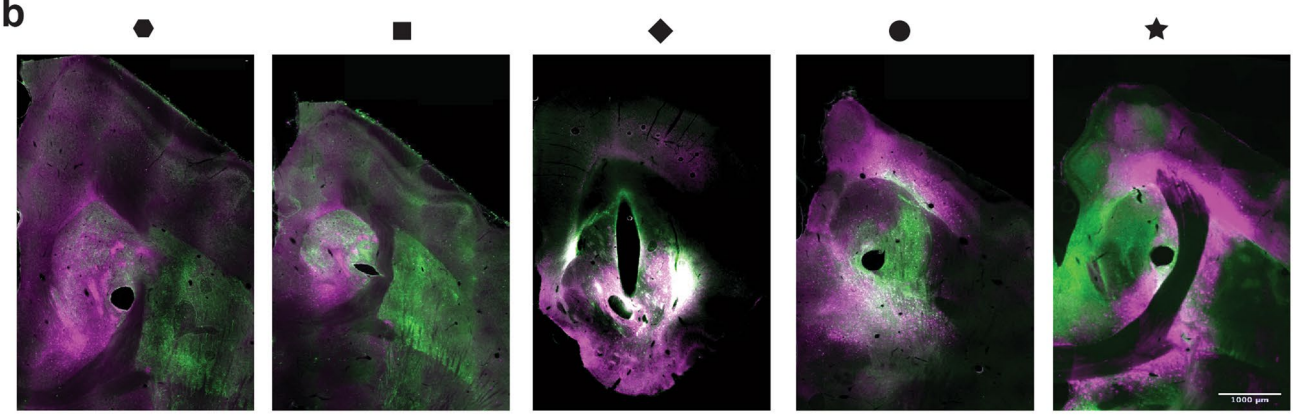

c

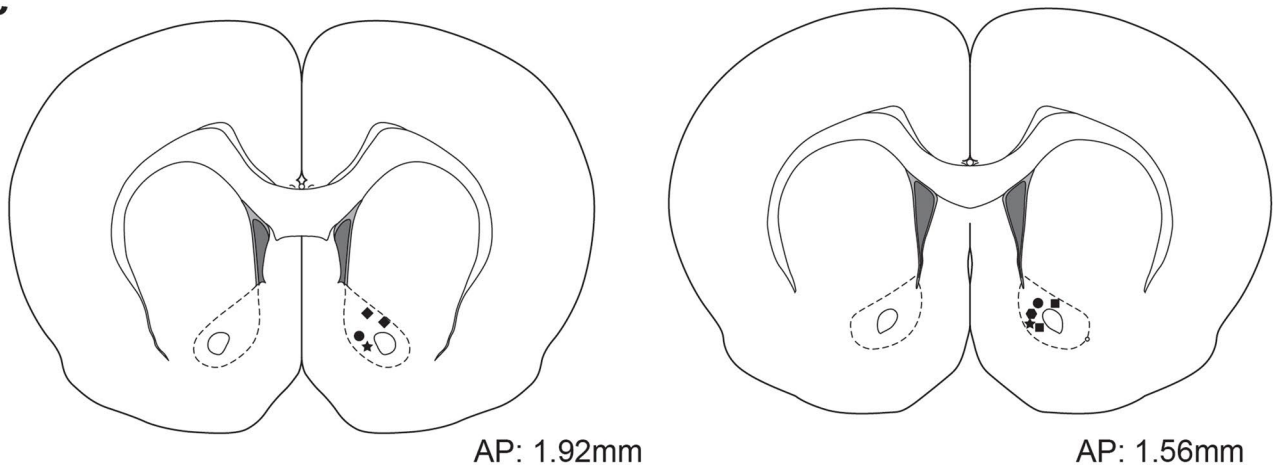

Extended Data Fig. 8 | Injection coordinates for in vivo experiments. a, List of all in vivo experiments in which RdLight1 was expressed in NAc simultaneously with a green indicator. **b**, Representative stitched image for each experiment collected on an epifluorescence microscope using a 4x objective. All sections (except for the *D1-Cre* example) are collected in horizontal planes. The *D1-Cre* example is in the coronal plane. Each section shows the most ventral section with a fiber punch hole. Scale bar: 1 mm. **c**, Overlaid reconstruction map of the estimate location of recordings for each experiment. Histology results were not available for one subject in the *TH-Cre* experiment since the subject died prior to the end of the experiment. Brain atlas outlines in this figure were reproduced with permission from (Paxinos and Watson, 2005).

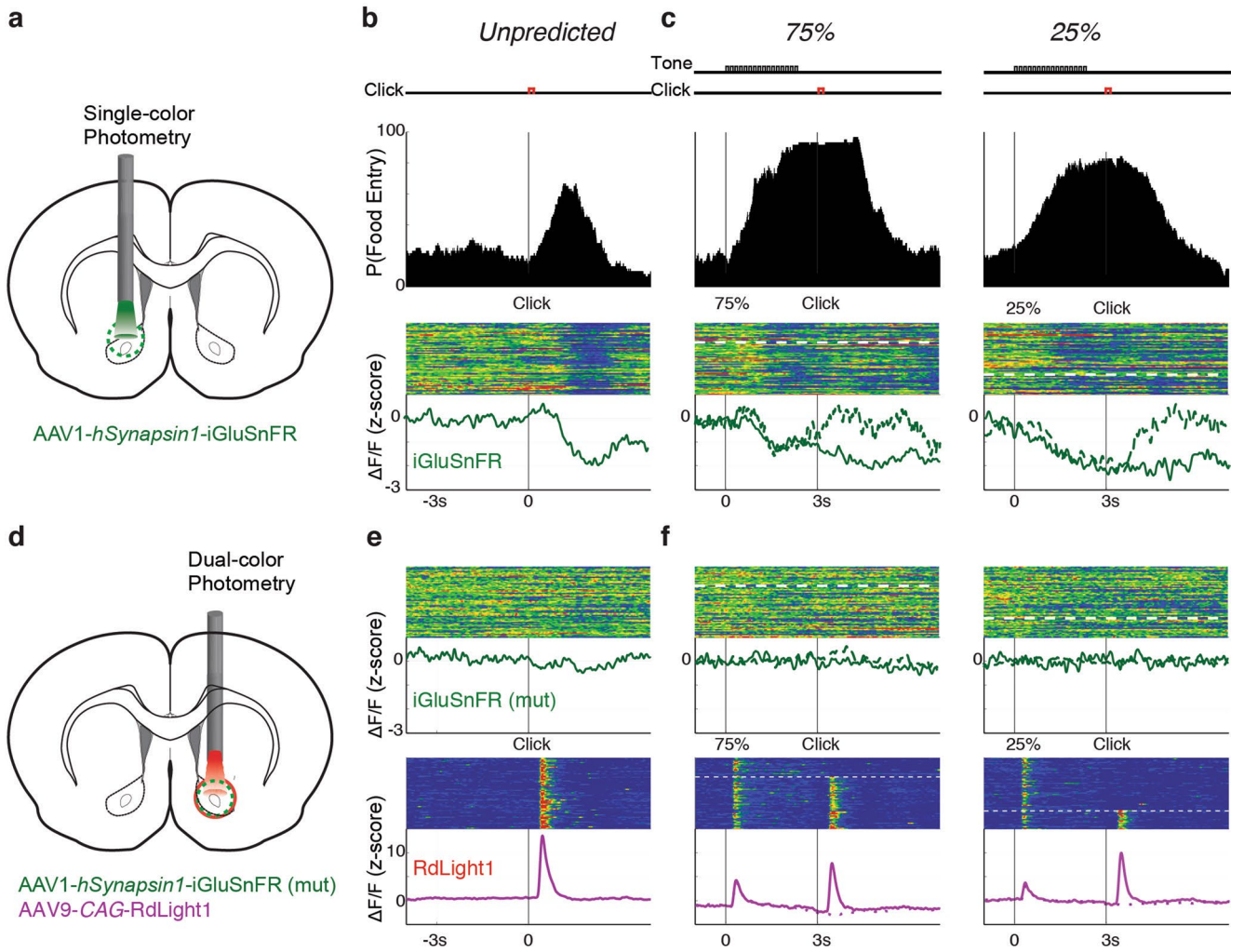

Extended Data Fig. 9 | Additional control experiments for in vivo imaging with iGluSnFR. To further validate the dip observed in the glutamate signal in NAc following the reward click in Fig. 4, we performed two complementary experiments. **a**, Only iGluSnFR was expressed in NAc and imaged using a 400 μm fiber during the pavlovian approach task. **b**, **c**, similar patterns to Fig. 4b,c, demonstrating a dip following the reward click was observed when only iGluSnFR was expressed and monitored. **d**–**f**, To control for pH changes or other artifacts, we expressed a variant of iGluSnFR (SF-iGluSnFR.R75A) with a mutation to the binding sites that destroyed glutamate binding, along with RdLight1. While similar to Fig 4b,c RdLight1 signal was preserved, the dip in the glutamate signal disappeared. Experiments for each panel were repeated independently for n=2 rats with similar results.

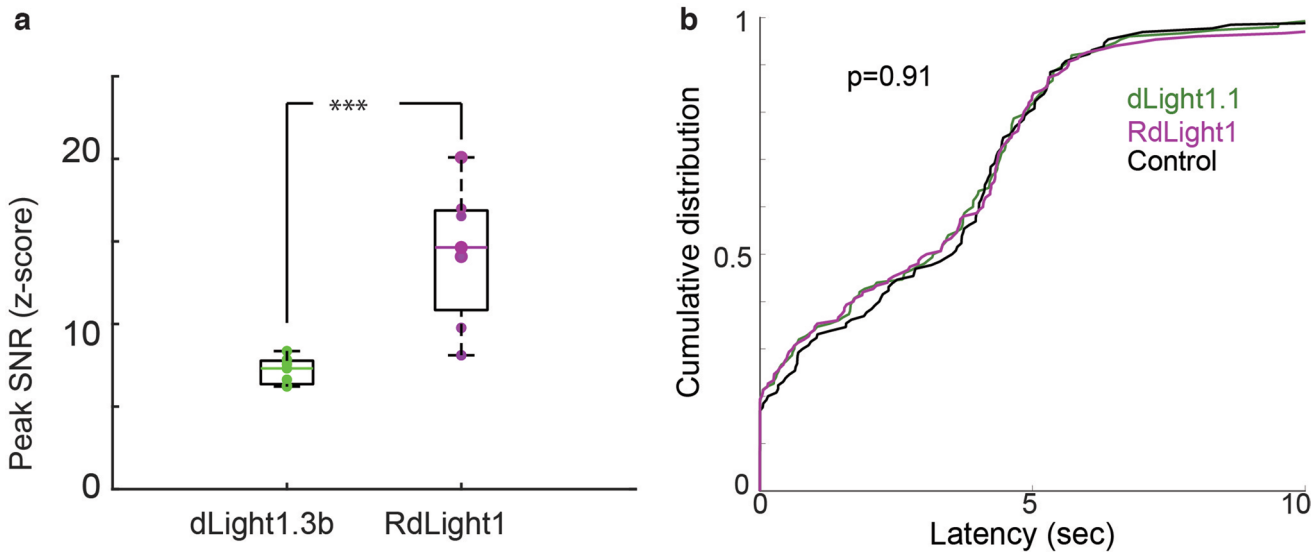

Extended Data Fig. 10 | In vivo signal-to-noise ratio comparison between RdLight1 and dLight1.3b, and effect of dLight1.1 or RdLight1 expression in NAc on motivated approach behavior. a, Peak response to an unpredicted click signaling immediate reward delivery. Signals were collected using fiber photometry across n=6 rats with dLight1.3b expressed in NAc and n=7 rats with RdLight1 expressed in the same coordinates. RdLight1 signals demonstrated significantly higher signal-to-noise ratio (SNR). A one-sided t-test was used to assess statistical significance (p=8.04x10^-3). Box plot shows the mean and quartiles of the data with whiskers representing the range of observations. **b**, To investigate the effect of dopamine indicators on behavior, we compared two cohorts of rats expressing either dLight1.1 (n=8) or RdLight1 (n=6) in NAc to a control group (n=6) expressing neither. Similar to the experimental paradigm for the in vivo photometry experiments, rats are placed in an operant chamber with a speaker and a reward delivery port. An auditory click indicating an immediate delivery of a sucrose pellet is played at random intervals. Rats with either of the indicators expressed in NAc show no difference to the control group in their latency to approach and retrieve the reward following the click. A kolmogorov-smirnov test was used to compare the latency distributions.

nature research

Corresponding author(s): Lin Tian, Joshua Berke, Mark von Zastrow

Last updated by author(s): May 21, 2020

Reporting Summary

Nature Research wishes to improve the reproducibility of the work that we publish. This form provides structure for consistency and transparency in reporting. For further information on Nature Research policies, see Authors & Referees and the Editorial Policy Checklist.

Statistics

For all statistical analyses, confirm that the following items are present in the figure legend, table legend, main text, or Methods section.

n/a	Confirmed	
☐	☒	The exact sample size (*n*) for each experimental group/condition, given as a discrete number and unit of measurement
☐	☒	A statement on whether measurements were taken from distinct samples or whether the same sample was measured repeatedly
☐	☒	The statistical test(s) used AND whether they are one- or two-sided *Only common tests should be described solely by name; describe more complex techniques in the Methods section.*
☒	☐	A description of all covariates tested
☒	☐	A description of any assumptions or corrections, such as tests of normality and adjustment for multiple comparisons
☐	☒	A full description of the statistical parameters including central tendency (e.g. means) or other basic estimates (e.g. regression coefficient) AND variation (e.g. standard deviation) or associated estimates of uncertainty (e.g. confidence intervals)
☐	☒	For null hypothesis testing, the test statistic (e.g. *F*, *t*, *r*) with confidence intervals, effect sizes, degrees of freedom and *P* value noted *Give P values as exact values whenever suitable.*
☒	☐	For Bayesian analysis, information on the choice of priors and Markov chain Monte Carlo settings
☒	☐	For hierarchical and complex designs, identification of the appropriate level for tests and full reporting of outcomes
☒	☐	Estimates of effect sizes (e.g. Cohen's *d*, Pearson's *r*), indicating how they were calculated

Our web collection on statistics for biologists contains articles on many of the points above.

Software and code

Policy information about availability of computer code

Data collection	Below is the software used for data collection in this manuscript: • Zeiss Zen 7, Zen (https://www.zeiss.com/microscopy/int/products/microscope-software/zen-lite.html) • Scanimage 5 (http://scanimage.vidriotechnologies.com/display/SIH/ScanImage+Home)
Data analysis	Below is the software used for data analysis in this manuscript: • ImageJ version1.52 (http://imagej.nih.gov/ij/download.html) • Matlab (https://www.mathworks.com/products/matlab.html) • IgorPro 8 (https://www.wavemetrics.com/order/order_igordownloads.htm) • GraphPad Prism 6 • flowCore package • R package version 1.52.1

For manuscripts utilizing custom algorithms or software that are central to the research but not yet described in published literature, software must be made available to editors/reviewers. We strongly encourage code deposition in a community repository (e.g. GitHub). See the Nature Research guidelines for submitting code & software for further information.

Data

Policy information about availability of data

All manuscripts must include a data availability statement. This statement should provide the following information, where applicable:

- Accession codes, unique identifiers, or web links for publicly available datasets
- A list of figures that have associated raw data
- A description of any restrictions on data availability

Raw data and custom written code can be made available upon request.

Field-specific reporting

Please select the one below that is the best fit for your research. If you are not sure, read the appropriate sections before making your selection.

☒ Life sciences ☐ Behavioural & social sciences ☐ Ecological, evolutionary & environmental sciences

For a reference copy of the document with all sections, see nature.com/documents/nr-reporting-summary-flat.pdf

Life sciences study design

All studies must disclose on these points even when the disclosure is negative.

Sample size	No sample size calculation was performed. Based on previous publications, in vitro experiments were performed in triplicate unless otherwise noted.
Data exclusions	No data were excluded from analysis for in vitro assays. In vivo data were excluded only when no photometry signal was observed.
Replication	Each experiment was performed on multiple cultures or animal subjects.
Randomization	Animals and cultures were randomly assigned for transduction with the different constructs described in the manuscript.
Blinding	Blinding was not used and is not necessary in this study, because only one sensor RdLight1 is tested.

Reporting for specific materials, systems and methods

We require information from authors about some types of materials, experimental systems and methods used in many studies. Here, indicate whether each material, system or method listed is relevant to your study. If you are not sure if a list item applies to your research, read the appropriate section before selecting a response.

Materials & experimental systems

n/a	Involved in the study
☐	☒ Antibodies
☐	☒ Eukaryotic cell lines
☒	☐ Palaeontology
☐	☒ Animals and other organisms
☒	☐ Human research participants
☒	☐ Clinical data

Methods

n/a	Involved in the study
☒	☐ ChIP-seq
☐	☒ Flow cytometry
☒	☐ MRI-based neuroimaging

Antibodies

Antibodies used	Alexa-647-conjugated M1 antibody (1:1000): mouse monoclonal anti-FLAG antibody from Sigma (cat#3040) in-house conjugated to Alexa-647
Validation	Validated for IHC by the von Zastrow lab [Irannejad, R. et al. Nature 495, 534–538 (2013)].

Eukaryotic cell lines

Policy information about cell lines

Cell line source(s)	HEK293T (ATCC cat. no. 3216), U2OS (ATCC, cat. no. HTB-96)
Authentication	The cell lines were authenticated by the vendor (ATCC) using Short Tandem Repeat (STR) Profiling to detect misidentified, cross-contaminated, or genetically drifted cells.
Mycoplasma contamination	The cell lines used were mycoplasma-free.
Commonly misidentified lines (See ICLAC register)	No misidentified cell lines were used in this manuscript.

Animals and other organisms

Policy information about studies involving animals; ARRIVE guidelines recommended for reporting animal research

Laboratory animals	For ex vivo experiments, 6-18 week old wild-type mice (mus musculus, C57/Bl6 strain) of both sexes were used. For in vivo experiments we used 8-12 month old Long Evans rats of both sexes, either wild-type or TH:Cre, bred in the Berke Lab.
Wild animals	No wild animals were used in this manuscript.
Field-collected samples	No field collected samples were used in this manuscript.
Ethics oversight	The animal experiments were reviewed and approved by the Institutional Animal Care and Use Commitee (IACUC) of the University of California Davis and the University of California San Francisco.

Note that full information on the approval of the study protocol must also be provided in the manuscript.

Flow Cytometry

Plots

Confirm that:

☒ The axis labels state the marker and fluorochrome used (e.g. CD4-FITC).

☒ The axis scales are clearly visible. Include numbers along axes only for bottom left plot of group (a 'group' is an analysis of identical markers).

☐ All plots are contour plots with outliers or pseudocolor plots.

☐ A numerical value for number of cells or percentage (with statistics) is provided.

Methodology

Sample preparation	Three 60mm dishes of 0.4 million HEK 293T cells were transected with 1) 200 ng of pCMV-nLight1.3 and 200 ng of pCMV-RdLight1 (cotransfection), 2) 200 ng of pCMV-nLight1.3 and 200 ng of pCMV blank vector (nLight only), 3) 200 ng of pCMV-RdLight1 and 200 ng of pCMV black vector (RdLight only). After 48 hours, the cells were lift up and were run on FACScan.
Instrument	BECTON DISCKINSON FACScan
Software	Flowcore
Cell population abundance	The entire population was used since this experiment was intended to compare fluorescence intensity among different population of cells
Gating strategy	No gating was applied since this experiment was intended to compare fluorescence intensity among different population of cells.

☐ Tick this box to confirm that a figure exemplifying the gating strategy is provided in the Supplementary Information.